Article

Molecular Cell

Toxicity of Eosinophil MBP Is Repressed by Intracellular Crystallization and Promoted by Extracellular Aggregation

Graphical Abstract

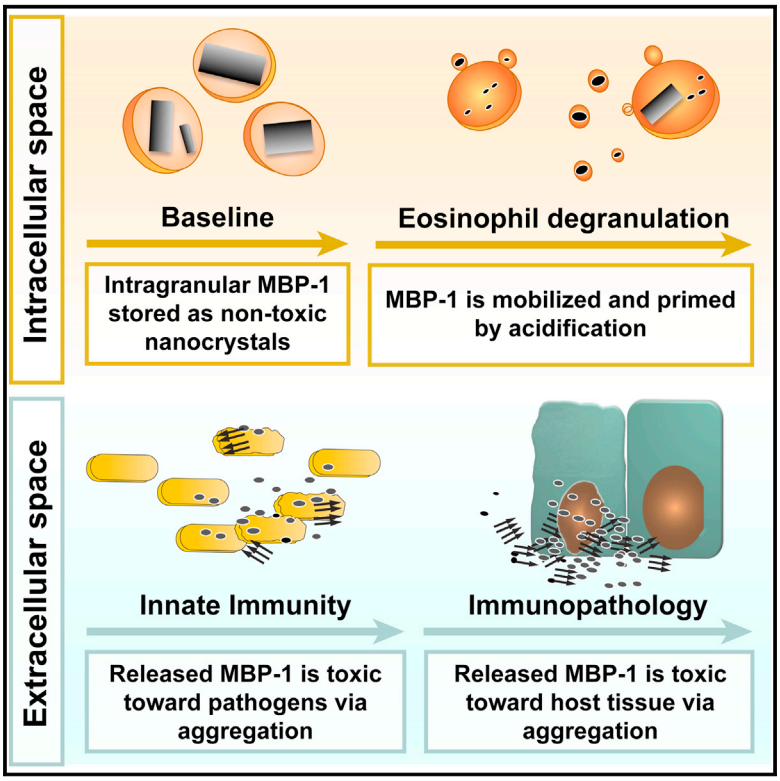

Highlights

- MBP-1 toxicity is restrained via crystallization in eosinophil secretory granules
- The nanocrystals are amenable to structural characterization using XFEL radiation
- MBP-1 amyloidogenic aggregation mediates toxicity toward pathogens and host cells
- Bulky extracellular plaques limit immunopathology in eosinophil-infiltrated organs

Authors

Alice Soragni, Shida Yousefi, ..., David S. Eisenberg, Hans-Uwe Simon

Correspondence

roland.riek@phys.chem.ethz.ch (R.R.), hus@pki.unibe.ch (H.-U.S.)

In Brief

MBP-1 is a powerful toxin secreted by eosinophils as part of the innate immune response against pathogens that can also cause tissue damage in eosinophilic diseases. Soragni et al. show how MBP-1 crystallization and amyloidogenic aggregation regulate its toxicity toward pathogens and host cells.

Accession Numbers

4QXX

Soragni et al., 2015, Molecular Cell *57*, 1011–1021
March 19, 2015
http://dx.doi.org/10.1016/j.molcel.2015.01.026

Molecular Cell
Article

Toxicity of Eosinophil MBP Is Repressed by Intracellular Crystallization and Promoted by Extracellular Aggregation

Alice Soragni,[1,2,3] Shida Yousefi,[2] Christina Stoeckle,[2] Angela B. Soriaga,[1] Michael R. Sawaya,[1] Evelyne Kozlowski,[2] Inès Schmid,[2] Susanne Radonjic-Hoesli,[2] Sebastien Boutet,[4] Garth J. Williams,[4] Marc Messerschmidt,[5] M. Marvin Seibert,[4] Duilio Cascio,[1] Nadia A. Zatsepin,[6] Manfred Burghammer,[7,8] Christian Riekel,[7] Jacques-Philippe Colletier,[9,10,11] Roland Riek,[3,12,*] David S. Eisenberg,[1,12] and Hans-Uwe Simon[2,12,*]
[1]UCLA-DOE Institute, HHMI, and Departments of Biological Chemistry and Chemistry and Biochemistry, 611 Charles E. Young Drive, University of California, Los Angeles, Los Angeles, CA 90095-1570, USA
[2]Institute of Pharmacology, University of Bern, Friedbuehlstrasse 49, 3010 Bern, Switzerland
[3]Department of Physical Chemistry, ETH Zurich, Wolfgang-Pauli-Strasse 10, 8093 Zurich, Switzerland
[4]Linac Coherent Light Source (LCLS), SLAC National Accelerator Laboratory, 2575 Sand Hill Road, Menlo Park, CA 94025
[5]National Science Foundation BioXFEL Science and Technology Center, 700 Ellicott Street, Buffalo, NY 14203, USA
[6]Department of Physics, Arizona State University, Tempe, AZ 85287, USA
[7]European Synchrotron Radiation Facility (ESRF), rue Jules Horowitz, 38043 Grenoble Cedex, France
[8]Department of Analytical Chemistry, Ghent University, Krijgslaan 281, S12B, 9000 Ghent, Belgium
[9]University Grenoble Alpes, IBS, 38044 Grenoble, France
[10]CNRS, IBS, 38044 Grenoble, France
[11]CEA, IBS, 38044 Grenoble, France
[12]Co-senior author
*Correspondence: roland.riek@phys.chem.ethz.ch (R.R.), hus@pki.unibe.ch (H.-U.S.)
http://dx.doi.org/10.1016/j.molcel.2015.01.026

SUMMARY

Eosinophils are white blood cells that function in innate immunity and participate in the pathogenesis of various inflammatory and neoplastic disorders. Their secretory granules contain four cytotoxic proteins, including the eosinophil major basic protein (MBP-1). How MBP-1 toxicity is controlled within the eosinophil itself and activated upon extracellular release is unknown. Here we show how intragranular MBP-1 nanocrystals restrain toxicity, enabling its safe storage, and characterize them with an X-ray-free electron laser. Following eosinophil activation, MBP-1 toxicity is triggered by granule acidification, followed by extracellular aggregation, which mediates the damage to pathogens and host cells. Larger non-toxic amyloid plaques are also present in tissues of eosinophilic patients in a feedback mechanism that likely limits tissue damage under pathological conditions of MBP-1 oversecretion. Our results suggest that MBP-1 aggregation is important for innate immunity and immunopathology mediated by eosinophils and clarify how its polymorphic self-association pathways regulate toxicity intra- and extracellularly.

INTRODUCTION

Eosinophils are highly specialized effector cells with multiple immunoregulatory functions (Rosenberg et al., 2013). As effector cells, they participate in the innate immune response against bacteria, viruses, and helminths by secreting highly cytotoxic proteins contained within their secretory granules. In addition, eosinophils play an essential role in the pathogenesis of various inflammatory and neoplastic disorders (Simon and Simon, 2007). After transendothelial migration, they can invade target organs, where they release inflammatory mediators, including their cytotoxic proteins, thereby participating in the inflammatory processes with tissue damage and subsequent remodeling (Kita, 2011).

Eosinophils store four toxic proteins in their specific granules: two ribonucleases (eosinophil cationic protein [ECP] and eosinophil-derived neurotoxin [EDN]/RNase2), a peroxidase (eosinophil peroxidase [EPO]), and the eosinophil major basic protein 1 (MBP-1) (Kita, 2011). In addition, MBP-2, a less potent homolog of MBP-1 with fewer positively charged residues, is also present (Plager et al., 1999). Upon release, cytotoxic granule proteins are found in association with mtDNA (Yousefi et al., 2008), in extracellular granule deposits, or in association with collagen fibers in eosinophilic tissues (Simon et al., 2011). ECP and EDN/RNase2 exert their full toxicity by a combination of post-activation processing and internalization (Plager et al., 2009; Woschnagg et al., 2009), whereas EPO requires an appropriate substrate to generate toxic oxidizers (Slungaard and Mahoney, 1991). MBP-1 is believed to exert its toxic effect by disrupting the membranes of parasites and bacteria (Abu-Ghazaleh et al., 1992a). Toxicity of MBP-1 toward host cells, such as bronchial epithelial cells in asthma, has also been reported (Frigas and Gleich, 1986). Clearly, this non-selective mechanism of toxicity has to be tightly controlled within the eosinophil itself and in the extracellular space to avoid cell lysis and host tissue damage.

Here we investigate how MBP-1 toxicity is controlled by crystallization and aggregation. We show how MBP-1 is packed in the specific granules of human eosinophils as a distinctive nanocrystalline structure, enabling the inert storage of the toxic protein. Using state-of-the-art X-ray-free electron laser (XFEL) radiation, we obtained unprecedented high-resolution diffraction patterns from MBP-1 nanocrystals probed in their cellular milieu. Additionally, we investigated how, within the innate immune response, MBP-1 gains its antibacterial properties via self-aggregation. Protein aggregation has long been considered as a deleterious process hampering cellular homeostasis. The association of protein aggregation with disease was established decades ago for disorders such as Alzheimer's or Parkinson's disease (Eisenberg and Jucker, 2012). On the other hand, functional protein self-association is being increasingly characterized in yeast, fungi, bacteria, algae, and humans (Fowler et al., 2007). Here we demonstrate how MBP-1 aggregation not only mediates its function within the innate immune system but also how it contributes to the immunopathology in eosinophilic diseases. Taken together, the results of this study highlight how MBP-1 self-association is regulated, providing a rationale for how the protein is stored, activated, and rendered toxic.

RESULTS

Structural Characterization of the MBP-1 Nanocrystals within the Granule Environment

Earlier transmission electron microscopy (TEM) work suggested that the ordered eosinophil granule cores are of a pseudocrystalline nature (Miller et al., 1966). To get direct evidence, we probed them with XFEL crystallography in their granule environment. Intact granules isolated from blood obtained from patients with hypereosinophilic syndromes (Valent et al., 2012) were deposited on a silicon wafer (Figures 1A–1C) mounted on an X-Y translation stage. We collected 1600 single frames, with 5.3% of the observed patterns categorized as single-crystal diffraction (Figures 1D and 1E; Figures S1A–S1D and S1F; Table S1). 10% of these were of sufficient quality to be indexed reliably. Despite drying the granules on the wafer, we could observe diffraction, indicative of well ordered crystals. This may be attributable to the protective action of the organelle surrounding the nanocrystals, preventing dehydration, or, potentially, to the small crystal solvent content.

The approximate unit cell parameters determined from a subset of interpretable images were a = 26.4 Å, b = 53.7 Å, and c = 58.8 Å, imposing orthorhombic symmetry with an estimated Matthews coefficient of 1.51 $Å^3$/Dalton and one MBP-1 molecule per asymmetric unit (Table S2). Although these unit cell parameters are most consistent with a primitive orthorhombic lattice, the nanocrystals may possess a primitive monoclinic lattice (P2 or $P2_1$; Figure 1F). The lattice has distinctly different parameters than the one determined for isolated and purified MBP-1 re-crystallized in vitro (Swaminathan et al., 2001; Figure 1F; Figures S1H and S1I). Interestingly, the granules also exhibited tinctorial properties typical of amyloid-like structures in both blood-purified as well as tissue-infiltrating eosinophils (Figure S2).

The nanocrystals did not contain heavy metals, as demonstrated by performing energy-dispersive X-ray analysis in combination with scanning TEM energy-dispersive X-ray (STEM-EDX) (Figure S3), different from insulin nanocrystals in pancreatic β cell granules which coordinate zinc (Dodson and Steiner, 1998).

The Crystalline Cores Act as Inert Deposits of the MBP-1 Toxin

MBP-1 has been shown to be a powerful toxin, broadly active toward a wide range of targets, including bacteria, helminths, and fungi (Acharya and Ackerman, 2014). Because of its ability to target different membranes, MBP-1 has to be stored safely within the granules. We hypothesized that the crystalline cores are able to lock the protein in a non-toxic conformation. Therefore, we measured the toxicity of MBP-1 cores in a bacterial killing assay (BKA) where purified nanocrystals were co-incubated with 0.5×10^7 *E. coli*/ml for 60 min before plating log dilutions. Intact MBP-1 nanocrystalline cores did not elicit significant cell death (Figure S4A), in support of the hypothesis that the crystals are able to lock the protein in a non-toxic conformation.

However, not only do eosinophils need to store MBP-1 in a safe way, but they must also trigger its toxicity when an infection occurs. Eosinophil activation is a complex process that includes granule acidification below pH 4 (Persson et al., 2002; Bankers-Fulbright et al., 2004). We tested whether a pH drop could rescue MBP-1 toxicity by equilibrating nanocrystals at various pH values (3, 4, 5.1, and 7.3), followed by BKA (Figure 2A). Only incubating cores at pH 3 consistently rescued MBP-1 toxicity, with bacterial viability reduced significantly down to ~10%.

We hypothesized that the difference in toxicity may arise from diverse amounts of solubilized MBP-1 at the various pH values (Abu-Ghazaleh et al., 1992b). After 30 min of incubation at either pH 3 or 7.3, we centrifuged the insoluble material and found that the protein released was two to three times more concentrated at pH 3 than at pH 7.3 (Figure 2B). Therefore, we repeated the BKA, correcting for the difference in concentration and observed that the supernatant derived from the acidic solubilization was still significantly more toxic (Figure 2B). These data suggest that, although some protein may be released from the cores at higher pH values, treatment at an acidic pH converts MBP-1 into a toxic-competent state.

The toxic-competent MBP-1 is of low molecular weight; filtering the soluble protein obtained upon acidic treatment through a 100-nm filter (Figure 2C) did not significantly diminish toxicity. This is compatible with monomeric or small oligomeric assemblies of MBP-1 with diameters below 0.1 μm being released from the nanocrystals upon activation.

Mechanism of Toxicity of MBP-1 and Aggregation Propensity In Vitro

It has been proposed that MBP-1 interacts with and disrupts membranes (Abu-Ghazaleh et al., 1992a). The broad and unspecific toxicity resembles certain amyloid toxins, such as Aβ oligomers or the antimicrobial peptide LL-37 (Soscia et al., 2010). This similarity, coupled with the remarkable insolubility of MBP-1 (Gleich et al., 1976), led us to hypothesize that the protein may exert its toxic effect via aggregation. We characterized the

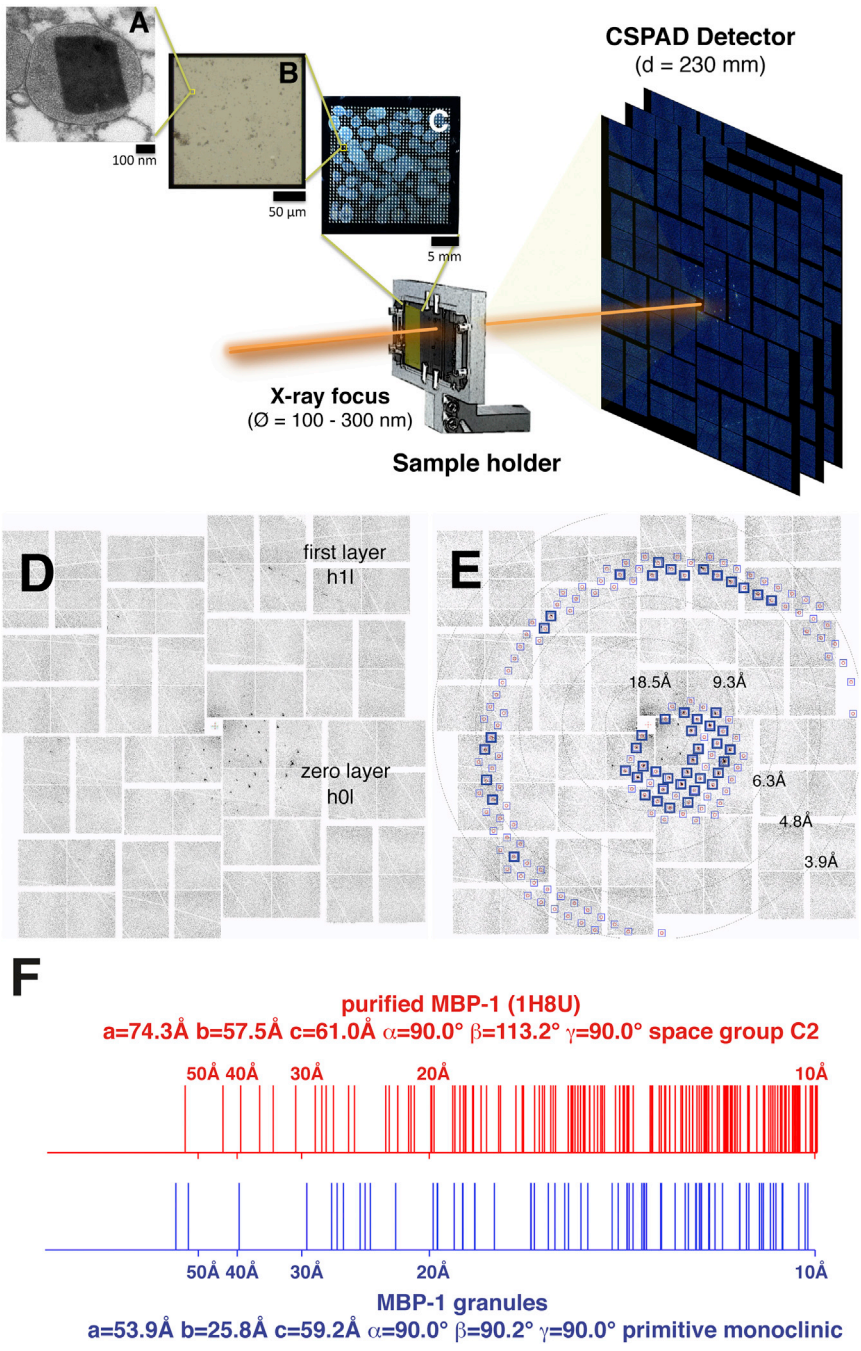

Figure 1. The Crystalline Nature of MBP-1 In Its Granule Environment

(A–C) Schematic of the experimental setup using XFEL in combination with fixed targets. The diameter of the X-ray beam (Ø) at the focal point was 100–300 nm full width at half maximum, whereas the sample-to-detector distance (D) was 230 mm. (A) TEM micrograph of a section of a resin-embedded granule showing an MBP-1 nanocrystal. (B) Magnification of a single 200 × 200 µm silicon nitride window surrounded by a silicon frame. Thousands of intact isolated granules are deposited on the surface. (C) A complete wafer.

(D) Diffraction patterns obtained when the XFEL beam intercepts a single MBP-1 nanocrystal within its cellular environment.

(E) Overlay of the observed diffraction spots with the predictions of the calculated lattice constants (blue boxes). The excellent agreement validates the lattice determination. Blue boxes highlight the predictions fulfilled by experimental data.

(F) Comparison of observed diffraction with lattice spacings of purified and recrystallized MBP-1 illustrating the differences between the two structures. Vertical lines mark the Bragg spacings (10–100 Å resolution) for two types of crystals: intragranular MBP-1 nanocrystals calculated from XFEL diffraction patterns and MBP-1 purified and recrystallized in vitro as calculated from PDB ID code 1H8U.

aggregation properties of MBP-1 in detail. We pinpointed several aggregation-prone regions using ZipperDB, an algorithm capable of identifying segments with a high likelihood to form steric zippers, pairs of β sheets that form the spines of amyloid fibers (Sawaya et al., 2007; Goldschmidt et al., 2010). These include residues 9–14, 26–38, 41–54, and 89–97 (Figure 3A). When mapped onto the in vitro crystal structure of MBP-1 (Swaminathan et al., 2001), most segments are solvent-exposed (Figure 3B). We determined the atomic structure of the five-residue segment predicted to have the highest amyloid propensity ($MBP\text{-}1_{26–30}$; sequence, GNLVS) to 1.5-Å resolution (Figure 3C; Table 1, PDB ID code 4QXX). The GNLVS segment formed a class four steric zipper in which β strands are stacked parallel, whereas β sheets are packed together via interdigitating hydrophobic side chains in a "face-to-back" orientation (Sawaya et al., 2007).

Full-length MBP-1 readily aggregated in solution over the entire range of pH values and reduction potentials tested (Figure 3D). We set up an aggregation assay in vitro starting with monomeric MBP-1 purified from eosinophils (see Experimental Procedures). After a 2 hr incubation of 0.2 mg/ml MBP-1 at 37°C with mild shaking, we detected aggregates by TEM under every condition tested (Figure 3D). The intrinsic instability of the protein was originally attributed to the formation of aberrant disulfide bridges (Gleich et al., 1976). However, the aggregation process we describe is independent of the presence of free cysteines, given that addition of 10 mM DTT did not significantly affect the rate of aggregation. The aggregates could be stained with Thioflavin T (ThioT) and luminescent conjugated polymers (pentamer formyl thiophene acetic acid [p-FTAA]) (Aslund et al., 2007), indicating the likelihood of a cross-β sheet architecture typical of amyloids (Figure S4B).

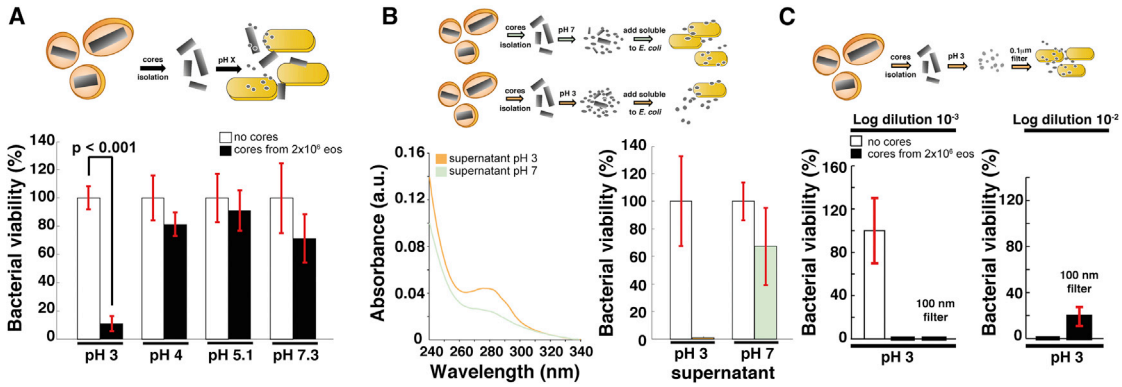

Figure 2. Mechanism of Generation of Toxic MBP-1 from Non-Toxic Cores

(A) BKA. Granule cores were resuspended in PBS at the indicated pH values to mimic the acidification process of the granules during eosinophil activation. Incubating the cores at pH 4 resulted in a significant rescue of toxicity in one trial. Values (mean levels ± % SD of one representative experiment, n = 3) are normalized to the buffer control.

(B) As measured by A_{280}, twice as much soluble protein was released from nanocrystals at pH 3 compared with pH 7.3 (left panel). On the right, BKA performed with protein released from the cores at pH 3 and 7 upon normalization by concentration.

(C) BKA. The material released from the cores at pH 3 was either unfiltered or filtered through a 100 nm filter. Both samples had similar toxicities. Values (mean levels ± % SD of a representative experiment) are normalized to the buffer control.

MBP-1 Aggregation Causes Bacterial Membrane Disruption and Death

Next we carried out a BKA using *E. coli* and purified soluble MBP-1, determining the effect of the protein on bacterial viability and morphology. MBP-1 is a powerful bactericidal toxin that reduced *E. coli* viability in a concentration-dependent fashion with an apparent half-maximal inhibitory concentration (IC_{50}) of ~18 nM (Figure S4C). MBP-1-treated bacteria were either lysed or presented local perturbations of their cell membranes, visible by TEM as big patches forming on the surface that eventually developed into severe membrane extrusions (Figure 4A), similar to the action of LL-37 or cecropin B (Oren et al., 1999). To test whether aggregation contributes to MBP-1 toxicity, we set out to interfere with the aggregation process by using conformation-specific antibodies (A11 and OC) capable of binding β sheet-rich oligomers and fibrils and neutralizing amyloid aggregate toxicity (Kayed et al., 2003, 2007). Cell viability was restored to ~50% when MBP-1 was co-incubated with either antibody but not control rabbit immunoglobulin G (IgG) (Figure S4D). The membrane damage was either reduced or absent (Figure 4A). Heparin, a known aggregation enhancer that has been reported to irreversibly bind MBP-1 (Swaminathan et al., 2001), neutralized its toxicity (Figure S4E).

We performed similar assays using intact blood-derived eosinophils. We activated freshly isolated eosinophils in vitro with interleukin-5 (IL-5) and complement factor 5a (C5a) and tested the resulting toxicity on *E. coli* (Yousefi et al., 2008). Although activated eosinophils killed bacteria efficiently, the addition of the amyloid-binding OC significantly inhibited this effect (Figure 4B), showing how the toxic effects of degranulation can be countered by interfering with protein aggregation.

MBP-1 Aggregation Causes Damage to Epithelial Cells In Vitro, In Vivo, and Ex Vivo

MBP-1 also exhibits toxicity toward host cells in eosinophilic asthma, Churg-Strauss syndrome (CSS), and other eosinophilic disorders. We set out to test whether MBP-1 aggregation also mediates the unwanted toxic effects on epithelial cells by using an MBP-1-derived peptide that recapitulates the full-length protein toxicity but is short enough to be synthesized chemically (Thomas et al., 2001). $MBP\text{-}1_{18–45}$ encompasses the highest aggregation propensity region of the protein (Figure 3) and has antibacterial properties (Thomas et al., 2001; Figure S5A). We tested the effects of the peptide on bronchial epithelial cells because damage to these is a defining feature of eosinophilic asthma (Holgate, 2011). Exposure of BEAS-2B human bronchial epithelial cells to $MBP\text{-}1_{18–45}$ resulted in induction of cell death in a concentration- (Figure 4C) and time-dependent manner (Figure S5B). A control peptide with reduced aggregation propensity had no effect in this assay. The cell death induced by $MBP\text{-}1_{18–45}$ was rapid and had morphological features of apoptosis, such as cell shrinkage, nuclear condensation, and fragmentation (Figure S5C). However, pharmacological inhibition of caspases by addition of (3S)-5-(2,6-difluorophenoxy)-3-[[(2S)-3-methyl-1-oxo-2-[(2 quinolinylcarbonyl)amino]butyl]amino]-4-oxo-pentanoic acid hydrate (Q-VD) did not prevent MBP-1-mediated death (Figure 4D; Figure S5C), pointing to the possibility that the cell death observed was a form of programmed necrosis, conceivably parthanatos (David et al., 2009). Both OC and heparin, a known aggregation enhancer that considerably accelerated $MBP\text{-}1_{18–45}$ aggregation (Figure S5D), significantly neutralized MBP-1 toxicity (Figure 4D). The same experiments performed using primary human bronchial epithelial cells gave similar results (Figure 4E).

To confirm the causative role of MBP-1 aggregation in immunopathology of eosinophilic diseases, we performed in vivo experiments by injecting $MBP\text{-}1_{18–45}$ into the dermis of mice, mimicking extracellular granule protein deposition as it occurs in eosinophilic skin diseases (Leiferman et al., 1985). Intradermal $MBP\text{-}1_{18–45}$ injection was followed by a thinning of the keratinocyte layer within 5 hr. The majority of the remaining keratinocytes demonstrated evidence of DNA fragmentation (Figure 4F).

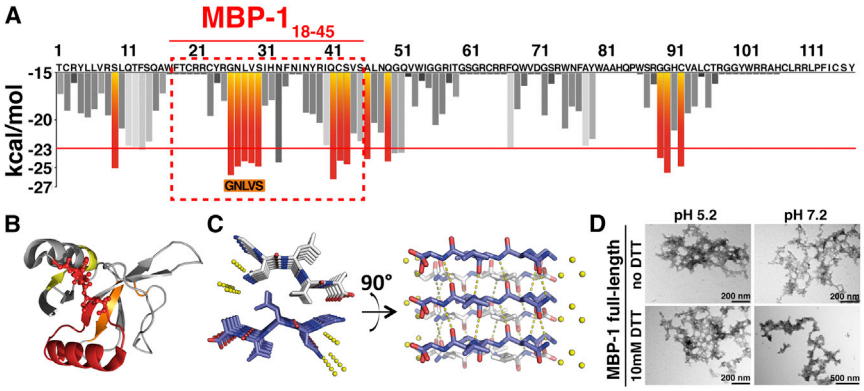

Figure 3. MBP-1 Amyloidogenic Properties

(A) Sequence-based prediction of MBP-1 aggregation propensity. The segments predicted to form an amyloid spine are in red.

(B) Aggregation-prone regions mapped onto the MBP-1 crystal structure. Predictions are based on the ZipperDB results. Aggregating residues (yellow/red) have predicted Rosetta energies below −23 kcal/mol. A stretch of aggregation-prone residues (26–54) forms a roughly continuous solvent-exposed area.

(C) X-ray structure of the amyloid zipper formed by the segment GNLVS (PDB ID code 4QXX). The amyloid is viewed down the fiber axis on the left and perpendicular to the fiber axis on the right. β sheets are shown in ivory and blue, water molecules in yellow, and hydrogen bonds as dotted lines.

(D) MBP-1 aggregates rapidly in solution under all tested conditions, as visible by TEM.

Application of MBP-$1_{18–45}$ together with OC or heparin completely neutralized the toxicity. We confirmed the results by using human skin ex vivo. Exposure of human skin explants to MBP-$1_{18–45}$ for 5 hr also induced DNA fragmentation in keratinocytes that could be blocked with both OC antibody and heparin (Figure 4F). Histological analysis revealed many small and irregularly shaped keratinocytes with pyknotic nuclei (Figure 4F, bottom).

Deposition of MBP-1 Amyloids in Eosinophilic Tissues

Massive eosinophil infiltration and degranulation is a defining feature of several inflammatory disorders, including atopic dermatitis (AD), CSS, and eosinophilic cellulitis (Wells' syndrome) in which extracellular MBP-1 deposits have been reported as part of the characteristic flame figures (Peters et al., 1983). We asked whether, in these diseases, MBP-1 aggregating extracellularly might form bulk deposits, similar to plaques in other protein aggregation diseases. To test this, we stained biopsies derived from eosinophilic patients with the amyloid-specific dye Congo Red (CR) and found several positive samples (Figure 5; Figure S6A). In a Wells' syndrome case, flame figures were stained by CR and showed apple-green birefringence, indicative of the presence of amyloids in serial sections (Figure 5B; Figure S7). The amyloid was formed, at least in part, by extracellular MBP-1, given the overlap with CR (Figure 5C), whereas no EPO (Figures 5D) or EDN/RNase2 (Figure S7) was found in the area. In agreement with observations published previously in AD (Leiferman et al., 1985) and eosinophilic endomyocardial disease (Wright et al., 2011), MBP-1 deposition could be observed in the absence of adjacent eosinophils, suggesting that the material may remain in tissues for extended periods of time. In other cases, amyloid aggregates were found adjacent to eosinophils in tissues obtained from AD (Figure S6B) and CSS patients (Figure S6C), suggesting that the extracellular amyloid material was generated by these cells.

DISCUSSION

Here we show that MBP-1 explores diverse modes of self-assembly, sampling different pathways to accomplish its diverse functions of inert storage or active toxin. This is possible because of MBP-1's highly basic and insoluble character coupled with its transition among various physicochemical environments. Based on our data and work published previously, we propose the following model for the production, storage, and action of MBP-1. During eosinophil differentiation, MBP-1 is produced as a 222-amino acid residue pre-protein that, because of the inhibitory function of the acidic N terminus, has no cytotoxic effect (Figure 6A). Conceivably, the N-terminal domain prevents pro-MBP-1 aggregation in vivo (DiScipio et al., 2011). During granule maturation, pro-MBP-1 is cleaved as the C-terminal region (106–222) starts to crystallize (Popken-Harris et al., 1998; Figure 6A). Given the high propensity of MBP-1 to aggregate at an intragranular pH (Figure 3D), it is clear that crystallization locks the protein, preventing intracellular toxicity (Figure 2C). In addition, the nanocrystals provide an efficient storage system to contain high concentrations of protein in a confined space. Hormones are stored in secretory granules as functional amyloid aggregates, a way to tightly pack a protein or peptide by reducing its water content (Maji et al., 2009). In this article, we show that the eosinophil granules also demonstrate tinctorial properties of amyloids (ThioT, p-FTAA, and CR) (Aslund et al., 2007; Eisenberg and Jucker, 2012) as well as a similar reactivity to conformation-specific antibodies (Kayed et al., 2007) (OC, Figure S2). In addition, they contain highly ordered nanocrystals (Figure 1; Figure S1C). These two findings may be consistent if aggregation and crystallization are simultaneous, resulting in an amyloid crystal. A steric zipper interface could act as a crystal contact, which is absent in the structure reported for purified MBP-1 crystallized in vitro. On the other hand, the two phenomena may be independent, giving rise to crystallized protein and aggregated material in close proximity. Alternatively, MBP-1 could be properly folded as a monomer, and its "amyloid-like" properties arise from some characteristic of the periodic crystalline arrangement, like specific stacking of charges.

The granule cores are well ordered, giving rise to diffraction spots by XFEL radiation (Figure 1). To date, details of protein structures and interactions have been determined by purifying and re-crystallizing them in vitro or removing them from their physiological environment. Here we show that an XFEL with

Table 1. Statistics of X-Ray Data Collection and Atomic Refinement for the Structure of the GNLVS Segment of MBP-1

Crystal Parameters	
Peptide sequence	GNLVS
PDB ID code	4QXX
Space group	$P2_12_12$
Cell Dimensions	
a, b, c (Å)	4.76, 16.18, 35.76
α, β, γ (°)	90.0, 90.0, 90.0
Molecules in asymmetric unit	1
Data Collection	
Synchrotron beamline	APS (24-ID-E)
Wavelength (Å)	0.9792
Unique reflections	638
Overall redundancy[a]	5.9 (5.5)
Completeness (%)[a]	98.7 (100)
$R_{merge(linear)}$ (%)[a,b]	11.3 (46.0)
$< I/\sigma I >$[a]	10.3 (4.94)
Refinement	
Resolution (Å)	17.88–1.44
R_{work} (%)[c]	16.4
R_{free} (%)[d]	19.2
Number of Atoms	
Protein	34
Ligand/ion	0
Water	3
Average B factor	8.2
Root-mean-square deviation	
Bond length (Å)	0.01
Bond angle (°)	1.27

[a]Values in brackets are for the highest-resolution shells.
[b]$Rmerge(linear) = \sum(|I - \langle I\rangle|)/\sum I$, where I is the observed intensity of the reflection HKL, and the sum is taken over all reflections HKL.
[c]$Rwork = \sum||F_o| - |F_c||/\sum|F_o|$.
[d]R_{free} as defined by Brünger, 1992, and calculated using 10% of the data.

beam cross-section matching the nano-sized protein crystals produces structural information from naturally occurring human nanocrystals within their physiological granule environment. The packing we observed from crystals probed in the granules differs from the crystals grown in the laboratory. This may arise from differences in the chemical environment in vivo versus in vitro, such as different pH values of crystallization or redox conditions that could influence MBP-1 conformation or packing.

After infection-triggered activation, eosinophils most frequently release their basic proteins by packaging them in vesicotubular compartments that are shuttled to the extracellular space (piecemeal degranulation; Figure 6C; Kita, 2011). During this process, the pH of the granules is acidified, enabling the disassembly of the crystalline core (Figure 2). Upon secretion, the change to a neutral pH favors MBP-1 conversion into an active cytotoxic entity able to bind and disrupt membranes (Figure 2; Figure S4). This could be a toxic amyloid oligomer formed in solution or a monomer that aggregates onto the bacterial surface. In either case, the protein would bind to the membrane and continue to aggregate to larger β sheet-rich clusters. Interestingly, ECP has also been reported to form amyloids that facilitate its antimicrobial activity (Torrent et al., 2012). Therefore, aggregation seems to be a shared mechanism facilitating toxicity of different eosinophil cationic proteins. In addition, several aggregation-prone segments are also present in MBP-2, including the 26–30 steric zipper. Therefore, MBP-2 may also undergo amyloidogenic aggregation, which can be facilitated further by the fewer positive charges present. Whether MBP-2 aggregation happens under physiological conditions and also mediates its functions remain to be established.

Toxic MBP-1 not only kills pathogens but also contributes to eosinophil-mediated immunopathology. In this article, we show how aggregation can mediate toxicity toward epithelial cells in vitro as well as in vivo when injected subcutaneously into mice or ex vivo on human skin explants (Figure 4). Our data show that interfering with the aggregation process either by addition of heparin or amyloid-binding antibodies can mitigate toxicity toward host cells (Figure 4; Figure S5). Heparin, which accelerates fibril formation (Figure S5), abolished MBP-1 toxicity, likely by rapidly converting smaller toxic aggregates into larger, inert deposits, pointing to a possible regulatory role of heparin-releasing mast cells under inflammatory conditions in which both cell types are present (Gilfillan and Beaven, 2011). These findings, together with the knowledge of which segments of the protein cause aggregation (Figure 3), may allow the generation of sequence-specific inhibitors with therapeutic potential in eosinophilic diseases (Sievers et al., 2011). Interestingly, drugs reported to interact with amyloids, such as chloroquine (Yang et al., 2005), amphotericin B (Hartsel and Weiland, 2003), and suramin (Levy et al., 2006), have been shown to provide beneficial effects in patients suffering from eosinophilic diseases (Newsome, 1987; Dereure and Guilhou, 2002; Ponikau et al., 2005), supporting our concept that functional MBP-1 amyloidogenesis is of pathophysiological relevance in eosinophil-mediated tissue damage and organ dysfunction.

On the other hand, when massive eosinophil infiltration and degranulation takes place, large MBP-1 amyloids accumulate extracellularly (Figure 5; Figure S7). These may have the beneficial effect of sequestering toxic oligomers as a negative feedback mechanism. This is in line with one of the proposed theories regarding Alzheimer's disease, namely that amyloid-β mature extracellular plaques have a protective role (Treusch et al., 2009; Eisenberg and Jucker, 2012). In addition, it has also been proposed that extracellular MBP-1 accumulation could function as a "junk mark" to recruit inflammatory cells (Lee and Lee, 2005). If MBP-1 amyloids are present (Figure 6; Figure S6), they may attract macrophages, which can be recruited to the site of amyloid deposition (Argilés et al., 2002). Therefore, MBP-1 extracellular aggregation into bulk non-toxic amyloids can be advantageous, providing a possible explanation for the observation that MBP-1 deposits can stay in tissues with relatively little evidence for tissue damage (Peters et al., 1983; Leiferman et al., 1985; Wright et al., 2011).

In summary, we demonstrate how MBP-1 is stored in inert ordered nanocrystals up to the point of its release, when

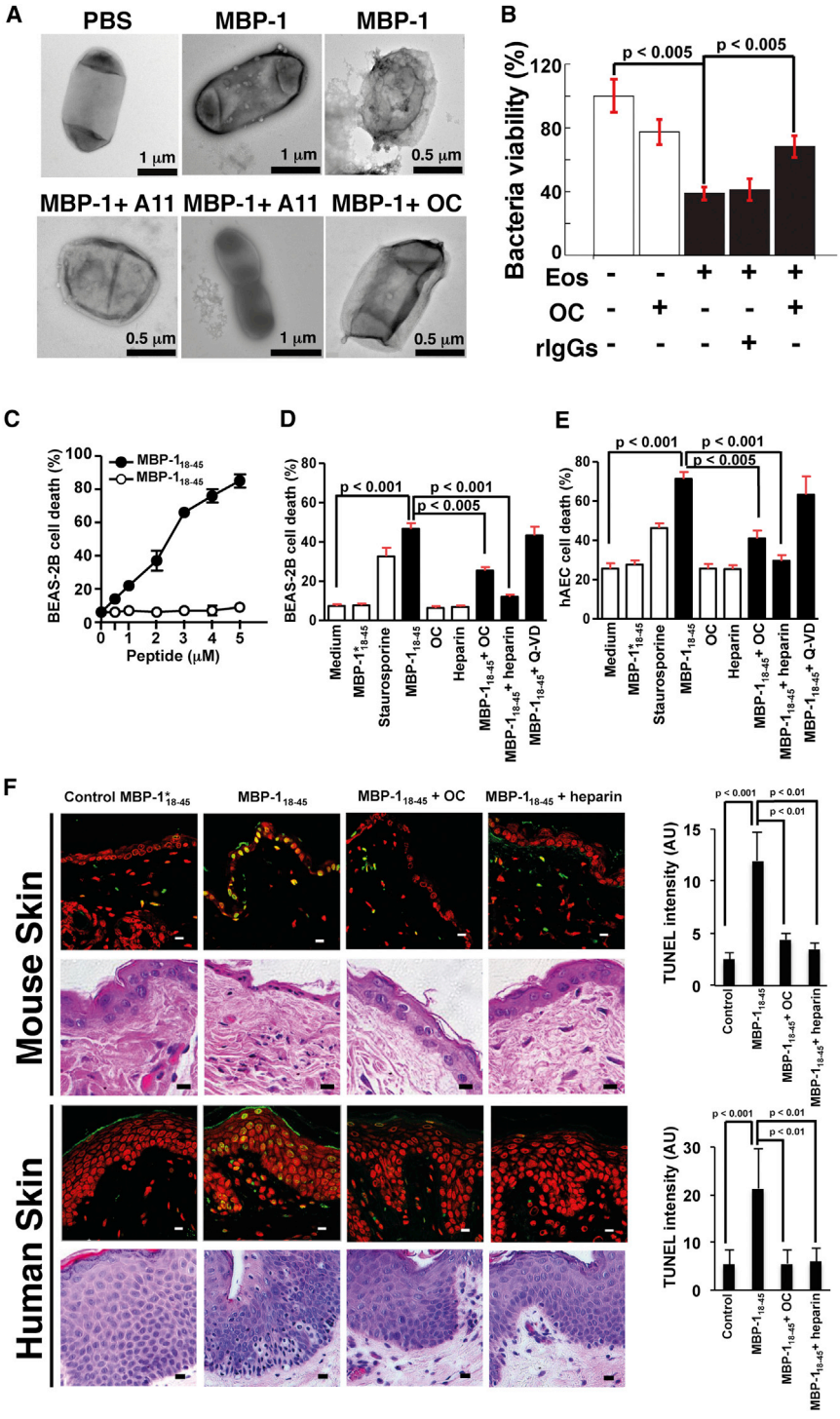

Figure 4. Aggregation Is Linked to MBP-1 Toxicity toward Invading Microorganisms and Host Cells In Vitro and In Vivo

(A) TEM picture of treated *E. coli*. Purified MBP-1, but not the PBS control, caused local perturbations on bacterial surfaces. Rescue of the observed phenotype is obtained by co-incubating MBP-1 with OC or A11 antibodies, thereby interfering with the aggregation process.

(B) BKA with activated blood-derived eosinophils. Activated eosinophils (Eos) significantly decreased bacterial viability, whereas addition of OC reduced toxicity. Log-dilutions of bacteria were plated in triplicates. Colony-forming unit counts are reported. Values (mean levels ± % SD of one representative experiment, n = 3) are normalized to the buffer control. rIgGs, rabbit IgGs.

(C) Toxicity of MBP-$1_{18–45}$ to the human bronchial epithelial cell line BEAS-2B is concentration-dependent (5 hr cultures).

(D) Toxicity of MBP–$1_{18–45}$ (5 μM) can be inhibited by OC or heparin. Staurosporine was used as positive control. Caspase inhibition by Q-VD did not prevent cell death.

(E) Similar results were obtained with primary human bronchial epithelial cells.

(F) Immunopathology mediated by MBP-$1_{18–45}$ (5 μM) and its inhibition by heparin or the amyloid-binding antibody OC. The peptides were injected into the dermis of mice or applied to human skin. Skin sections were analyzed by TUNEL assay (green). Nuclei were stained with propidium iodide (red). Statistical analysis was performed (mean levels ± % SD of three independent experiments). Skin sections were also analyzed by histology (bottom). In mice, MBP-$1_{18–45}$ reduced the numbers of keratinocytes. In human skin, application of the toxin resulted in pyknotic, shrunken, and irregularly shaped keratinocytes. AU, arbitrary unit.

amyloidogenesis triggers toxicity toward invading microorganisms, and provide in vitro, ex vivo, and in vivo evidence for MBP-1 aggregation as the mechanism behind MBP-1-mediated immunopathology as it occurs in eosinophilic diseases, such as hypereosinophilic syndromes, bronchial asthma, and AD. Our data validate functional crystallization and amyloidogenesis as regulatory mechanisms in the innate immune system.

EXPERIMENTAL PROCEDURES

Eosinophil Isolation

This study was approved by the Ethics Committee of the Canton of Bern. Human eosinophils were isolated from peripheral blood using the EasySep human eosinophil enrichment kit (STEMCELL Technologies) according to the manufacturer's instructions. Briefly, granulocytes were enriched by gradient centrifugation (Biocoll), and erythrocytes were lysed by hypotonic lysis. Eosinophils were then isolated by negative selection using a tetrameric antibody cocktail against CD2, CD3, CD14, CD16, CD19, CD20, CD36, CD56, CD123, and glycophorin A and dextran-coated magnetic particles. The resulting cell populations contained more than 99% eosinophils as controlled by staining with Diff-Quik (Medion) and light microscopy. It should be noted that, for the isolation of eosinophil cores and bacterial killing assays, isolation of eosinophils from hypereosinophilic donors was required.

Extraction of Granules and Nanocrystalline Cores

Granules were isolated as reported previously (Ohnuki et al., 2005). Briefly, eosinophils were lysed in 0.25 M sucrose (Sigma) with 250 U/ml heparin (catalog

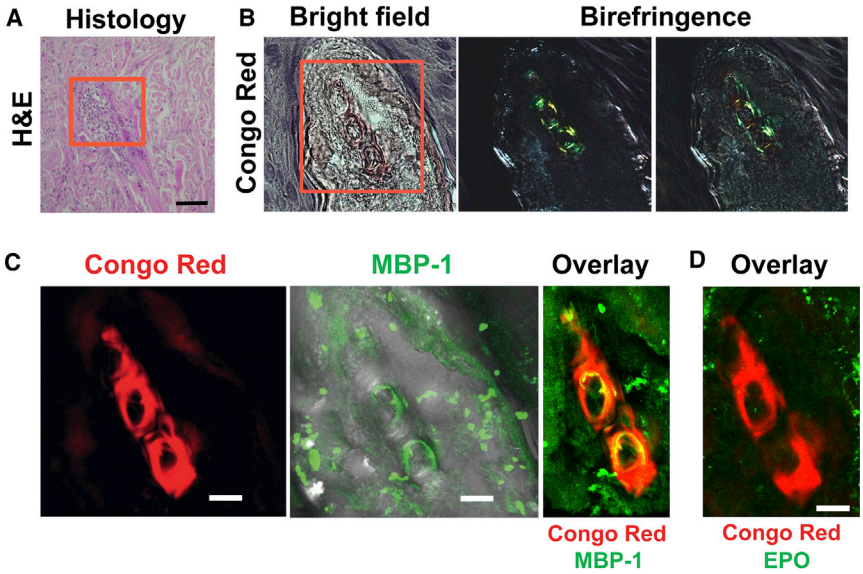

Figure 5. Extracellular MBP-1 Amyloid Deposits in Eosinophilic Tissue

(A) Skin biopsy from a Wells' syndrome patient. Histology shows typical collagen bundles; i.e., flame figures (red box). Scale bar, 100 μm.

(B) The area contains amyloids stained by Congo red that appear pale red in bright-field mode. When visualized between crossed polarizer and analyzer, yellow-green birefringence was present.

(C) Immunofluorescence analysis showed large extracellular MBP-1 deposition that partly overlapped with the CR fluorescence.

(D) In contrast, no EPO protein was detected.

no. H6279, Sigma) and processed with a mortar and pestle several times. Unbroken cells and debris were pelleted at 400 × *g* for 10 min, and the supernatant was then centrifuged for 20 min at 10,000 × *g* to collect the granules. To extract the cores, granules were lysed in 0.25 M sucrose with 0.1% Triton X-100 and disrupted using a glass mortar and pestle. The debris was pelleted at 400 × *g* for 10 min, and the supernatant containing the cores was deposited over a 50% sucrose cushion and pelleted at 20,000 × *g* for 30 min in an ultracentrifuge (Beckman Coulter Optima XL). The cores were resuspended in PBS.

XFEL

Measurements were performed by pipetting intact granules derived from ~30 million cells resuspended in water on a 25 × 25-mm wafer constituted of 30-nm thick, 200 × 200-μm Si_3N_4 membranes with a 200-μm-thick silicon frame as a support (Silson). Different sample concentrations were applied to the membrane to ensure optimal coverage while avoiding overlapping granules, which would give powder X-ray diffraction patterns rather than single-crystal patterns. The excess of water was air-dried before inserting the support in the vacuum chamber. Each window was shot once with a pulse of 50 fs using a 100–300 nm full width at half maximum (FWHM) beam in single shot mode. The experiment was performed at the Coherent X-Ray Imaging (CXI) beamline at the Linac Coherent Light Source (LCLS) (Boutet and Williams, 2010) using a tiled 2D pixel array detector (PAD) with 14-bit in-pixel digitization (Hart et al., 2012). Diffraction data were recorded using a 100–300 nm FWHM beam with a photon energy of 8.45 KeV (1.47 Å). The detector was positioned 230 mm from the sample. At total of 1,600 frames were recorded in 120 min. Approximate unit cell parameters were determined from a subset of interpretable images using Denzo (Otwinowski and Minor, 1997).

MBP-1 In Vitro Aggregation

For the aggregation experiments, aliquots of 400 μl of MBP-1 in 20 mM sodium acetate buffer with 150 mM NaCl at 0.2 mg/ml were prepared in three separate low-retention tubes, and the pH values were adjusted to 5.2, 7.3, and 11, respectively, by addition of sodium hydroxide. Each aliquot was divided into two, and one per pH condition was supplemented with 10 mM DTT. The tubes were placed in an Eppendorf thermomixer at 37°C and 800 rpm. After 2 hr, all samples contained aggregates, as visible by electron microscopy (EM) (Figure 3).

Aggregation experiments with the 18–45 peptide were performed as follows. MBP-$1_{18–45}$ was dissolved in 100% DMSO and filtered through a 0.22-μm filter prior to use. A_{280} of duplicate samples was measured to estimate concentration. Aggregation was performed in Tris buffer, with or without heparin, in the presence of 10 mM DTT.

Transmission Electron Microscopy

Isolated granules or cores were deposited on carbon-coated copper or nickel grids (EM Science) glow-discharged previously. After three washes in milliQ water, the grids were stained for 15–30 s with filtered 2% uranyl acetate. Images were acquired in bright-field mode with an FEI Morgagni 268 operated at 100 kV or with a FEI Tecnai F30 FEG operated at 300 kV. STEM and selected area electron diffraction (SAED) by TEM were performed on the FEI Tecnai F30 FEG.

Bacteria Killing Assay with Purified MBP-1

For the purified MBP-1 or isolated cores, the assay was performed using the Gram-negative *E. coli* strain BL21* (Stratagene). Briefly, bacteria were grown overnight in Luria-Bertani (LB) medium without antibiotics, washed twice in sterile magnesium and calcium-free PBS, and diluted so that the absorbance at 550 nm was 0.02, corresponding to 10^7 cells/ml. The bacteria were mixed at a 1:1 ratio with the same volume of the samples, resulting in a final concentration of 0.5 × 10^7 bacterial cells/ml. For purified MBP-1, 0.02 μg of protein were diluted in PBS (72.4 nM final concentration after bacteria addition unless indicated otherwise), and antibodies (1 μg total) or heparin (50 U total) were added. The samples were prepared in low-retention tubes (Neptune Plastics) and incubated for 1 hr at 37°C in an Eppendorf thermomixer with mild shaking (800 rpm). Five microliters of five to seven serial dilutions were plated on agar LB plates without antibiotics and incubated at 37°C for 12 hr, and then colonies were counted.

Bacteria Killing Assay with Isolated Cores

For the assay with extracted cores, the crystalline MBP-1 entities were extracted as reported above, and the pellet after the sucrose cushion was resuspended in PBS at pH 7.2. Aliquots corresponding to 2 × 10^6 eosinophils were prepared in low-retention tubes, and the samples were spun at 20,000 × *g* for 20 min. After removing the supernatant, the pellets were resuspended in PBS buffer at the indicated pH (3, 4, 5.1, or 7.2) and incubated for 30 min at 37°C. The samples were diluted 1:4 in PBS at pH 7.2 and incubated for 5 min at 37°C before addition of the same volume of bacteria as reported above.

Bacteria Killing Assay with Eosinophils Activated In Vitro

The BKA using activated eosinophils was performed as reported previously (Yousefi et al., 2008) using DH5α cells. Statistical analysis was performed with a Mann-Whitney *U* test. The figures show mean levels ± SD or SEM, as indicated in the text. p values are indicated in the graphs.

Bacteria Killing Assay with MBP-$1_{18–45}$ Peptide

The BKA using MBP-$1_{18–45}$ peptide was performed following the protocol described above with minor modifications. MBP-$1_{18–45}$ stocks in 100% DMSO were filtered with a 0.22-μm spin filter and then diluted to the final concentrations in PBS at pH 7.2. Negative controls with the same amount of DMSO were performed. Samples were normalized to the controls. Median values for three replicates ± SEM were calculated with Prism 6 software.

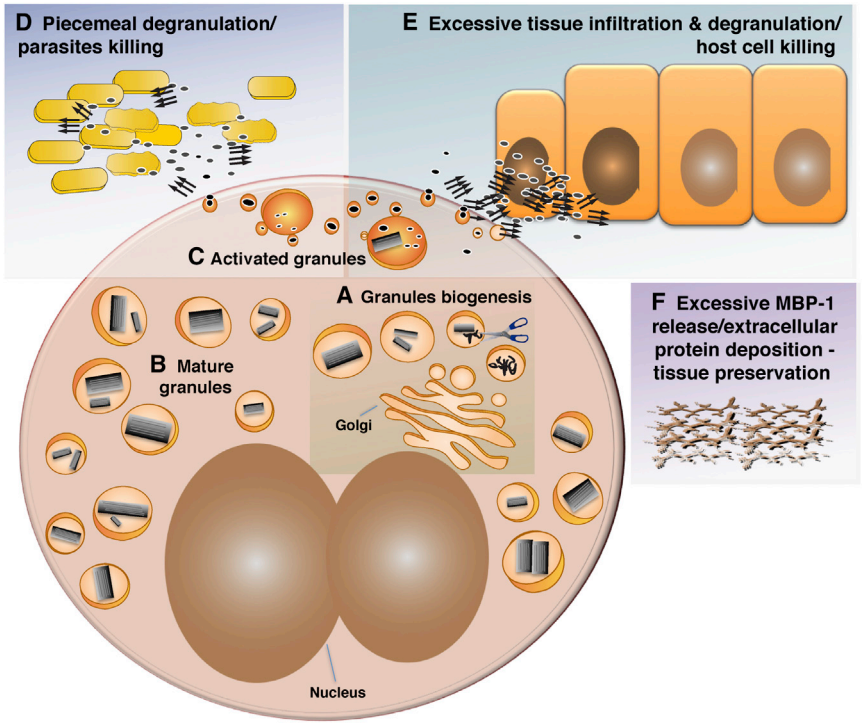

Figure 6. A Model for the MBP-1 Self-Association Cycle

(A) MBP-1 condensation begins before/at the same time of pro-protein processing in granules. The process is followed by compaction of the cores. Granule biogenesis occurs during eosinophil differentiation.

(B) A number of mature specific granules with a crystalline interior are dispersed in the cytosol.

(C) Following eosinophil activation, the granule pH drops, and the content is mobilized, unpacked, and released through secretory vesicles.

(D) MBP-1 exerts its antibacterial effect through aggregation.

(E) MBP-1 toxicity toward host cells is also mediated by aggregation.

(F) Under conditions of sustained activation and massive secretion of MBP-1, extracellular deposition of MBP-1 can take place. Parallel arrows indicate amyloid aggregates, scissors represent the unknown protease processing pro-MBP-1, and active and toxic MBP-1 are shown as gray ellipses.

Identification of Tissue MBP-1 Amyloids

Paraffin-embedded, 8-μm tissue sections from Wells' syndrome, atopic dermatitis, and CSS patients were deparaffinized and hydrated. We used the Congo red (CR) staining protocol of the HT-60 kit (Sigma) with minor modifications. Briefly, sections were washed three times in deionized water and stained for 1 min with Mayer's hematoxylin (Sigma). After washing for 2 min with tap water and three times with deionized water, the samples were placed in filtered alkaline NaCl solution for 20 min and then for 30 min in filtered alkaline CR staining solution. The slides were then washed twice with 95% ethanol and twice in 100% ethanol, cleaned in xylene, mounted with Dako fluorescent medium and imaged with an epifluorescence Zeiss 200M (inverse) microscope equipped with cross-polarizers. CR staining was followed by antibody staining. After the CR stain and imaging, the coverslips were removed, and the slides were left in PBS at 4°C for several days to allow the gradual release of the dye. The sections were then stained following the standard protocol and visualized by confocal laser microscopy (LSM 510 Exciter, Zeiss).

Immunofluorescence

Immunofluorescence staining was performed on freshly isolated and 4% paraformaldehyde-fixed eosinophils and 5-μm paraformaldehyde-fixed sections from eosinophilic esophagitis, CSS, and *Schistosoma*-infected patients (same as above). Immunofluorescence staining using primary antibodies directed to MBP-1 (catalog no. ab48372, Abcam) and OC (Millipore) and appropriately labeled secondary antibodies (Molecular Probes) was performed. Primary control antibodies served as negative controls. Analysis was performed by means of confocal laser-scanning microscopy (LSM 510).

Cells and Cell Cultures

BEAS-2B cells (a human bronchial epithelial cell line provided by Dr. Amiq Gazdhar, University of Bern) were grown in DMEM with 5% fetal bovine serum (FBS). Primary human airway epithelial cells of bronchial origin, hAECB, were purchased from Epithelix Sàrl and used at a low passage number after maintenance and passage according to the supplier's recommendations in a special medium (hAEC culture medium) not containing FBS.

One day prior to treatment with peptide, cells were trypsinized, seeded at 20,000 cells/100 μl using 96-well plates, and allowed to adhere overnight. The next day, adherent cells were washed three times with DMEM containing 17 mM 4-(2-hydroxyethyl)-1-piperazineethanesulfonic acid (HEPES) (pH 7.2–7.5) but without FBS to remove traces of FBS and incubated further in the same medium during the peptide treatment. MBP-$1_{18–45}$ or control peptide (Celtek or CSBio; MBP-$1_{18–45}$ sequence, FTCRRCYRGN LVSIHNFNIN YRIQCSVS; MBP-$1_{18–45}$ control peptide sequence, FTCRRCYRGN PVSIHPFNIN YRPQCSVS) at different concentrations with or without 5 μg/ml OC antibody (Millipore), 500 U/ml heparin (Sigma), or 20 μM pan-caspase inhibitor Q-VD (SM Biochemicals) was added to cells and incubated for the indicated times. 0.5 μM staurosporine (Sigma) was used as a positive control for induction of cell death.

Human and Mouse Skin Peptide Treatment

Human foreskin samples were obtained from Dr. Peter Klimek (Department of Pediatric Surgery, University Hospital Bern [Inselspital]). The study was approved by the ethics committee of the Canton of Bern. Any connective tissue was removed, and samples were cut into sterile 4-mm^2 pieces and incubated in DMEM containing 17 mM HEPES (pH 7.2–7.5) and 1% penicillin/streptomycin (Invitrogen) in the absence of FBS. Peptides (5 μM) in the absence or presence of OC antibody or heparin were added as described above and incubated for 5 hr. The skin tissues were placed in formalin solution overnight before paraffin-embedding and sectioning.

Animal experiments were reviewed and approved by the animal experimentation review board of the Canton Bern. For mouse experiments, 1 day before intradermal injection of peptide into C57BL/6 mice, animals were anesthetized using a mixture of 100 mg/kg ketamine and 10 mg/kg xylazine, and the fur on the back of the animals was shaved using an electric shaver. Subsequently, the skin was smoothed with a razor to remove any traces of fur without injury to the skin. The next day, the mice were again anesthetized, and the was skin sterilized with 70% ethanol and marked for the intradermal injection. A 50 μl Hamilton syringe was used for the intradermal injection of a total volume of 10 μl of peptide or a mixture of antibody and peptide or heparin and peptide. Peptides were used at 5 μM. The injection was made into the dermis of the mouse skin. Mice were sacrificed 5 hr after injection, and the injected area of skin was cut out using a sterile 3 mm skin punch and kept in formalin solution (Sigma) overnight before paraffin-embedding, sectioning, and staining.

TUNEL Assay

Tissue sections were deparaffinized and rehydrated, and microwave antigen retrieval was carried out. Cells grown on glass coverslips were fixed in 4%

formaldehyde in PBS (pH 7.4) and permeabilized in 0.1% Triton X-100 for 2 min on ice prior to performing the terminal deoxynucleotidyl transferase–mediated 2′-deoxyuridine 5′-triphosphate nick-end labeling (TUNEL) assay using a commercial kit (Roche). According to the supplier's protocol, the enzyme solution was diluted 1:50 in labeling solution, and 50 μl of this mixture was added to each sample. Incubation was performed for 60 min at room temperature. Following washing, nuclei were stained with Hoechst 33342 dye. All samples were mounted using Pro-Gold mounting medium.

ACCESSION NUMBERS

The RCSB PDB accession number for the MBP-$1_{26–30}$ structure reported in this paper is 4QXX.

SUPPLEMENTAL INFORMATION

Supplemental Information includes Supplemental Experimental Procedures, seven figures, and two tables and can be found with this article online at http://dx.doi.org/10.1016/j.molcel.2015.01.026.

AUTHOR CONTRIBUTIONS

A.S. designed the project, carried out most of the experiments, and wrote the manuscript with input from co-authors. S.Y. and I.S. performed the bacterial killing experiments and in vivo and ex vivo experiments. C.S. isolated blood eosinophils, performed in vitro work, and contributed ideas and comments. S.R.-H. isolated blood eosinophils. E.K. screened eosinophilic tissues for amyloid deposits and performed confocal microscopy work. A.B.S. determined the amyloid zipper structure. M.B. and C.R. performed the initial X-ray characterization of the granules at the nanofocused beamline ID-13 (ESRF, Grenoble, France). J.-P.C. contributed comments and ideas, participated in XFEL data acquisition, and processed the data. D.C. and M.R.S. participated in XFEL data acquisition and processed the data. N.A.Z. helped with XFEL data processing. S.B., G.J.W., M.M., and M.M.S. performed the XFEL experiment. R.R. provided comments and suggestions. D.S.E. designed and supervised the X-ray work and wrote the manuscript. H.-U.S. designed and supervised the in vitro, in vivo, and ex vivo work; provided tools and reagents; performed confocal microscopy work; and wrote the manuscript.

ACKNOWLEDGMENTS

We thank all patients and collaborating clinicians for providing blood and tissue samples for the research reported here. We thank M. Capel, K. Rajashankar, N. Sukumar, J. Schuermann, I. Kourinov, and F. Murphy at NECAT beamlines 24-ID at APS, which are supported by grants from the National Center for Research Resources (5P41RR015301-10) and the National Institute of General Medical Sciences (8 P41 GM103403-10) from the NIH. Use of the APS is supported by the DOE under Contract DE-AC02-06CH11357. We thank Matthias Frank, Mark S. Hunter, Michael J. Bogan, and John Miao for helpful experimental suggestions and scientific discussion; Anton Barty for help with XFEL image conversion and preliminary data analysis; and Stephan Stern and Tom Pardini for helping with the XFEL motor script. We thank the ESRF and LCLS staff for technical support. We acknowledge the EMEZ facility at ETH for support with the electron microscopy experiments, in particular Elisabeth Gruber-Miller, Fabian Gramm, and Peter Tittmann. We also acknowledge the use of instruments at the Electron Imaging Center for NanoMachines supported by NIH (1S10RR23057) and CNSI at UCLA. This work was supported by grants from the Swiss National Science Foundation (to R.R. and H.-U.S.); the National Science Foundation (MCB 1021557 to N.A.Z. and MCB 0958111 to D.S.E.); the Allergie-Stiftung Ulrich Müller-Gierok (to S.R.-H. and H.-U.S.); the German Research Foundation (to C.S.); and from the NIH (AG029430), the Keck Foundation, and HHMI (to D.S.E.).

Received: November 3, 2014
Revised: December 29, 2014
Accepted: January 20, 2015
Published: February 26, 2015

REFERENCES

Abu-Ghazaleh, R.I., Gleich, G.J., and Prendergast, F.G. (1992a). Interaction of eosinophil granule major basic protein with synthetic lipid bilayers: a mechanism for toxicity. J. Membr. Biol. *128*, 153–164.

Abu-Ghazaleh, R.I., Dunnette, S.L., Loegering, D.A., Checkel, J.L., Kita, H., Thomas, L.L., and Gleich, G.J. (1992b). Eosinophil granule proteins in peripheral blood granulocytes. J. Leukoc. Biol. *52*, 611–618.

Acharya, K.R., and Ackerman, S.J. (2014). Eosinophil granule proteins: form and function. J. Biol. Chem. *289*, 17406–17415.

Argilés, A., García García, M., and Mourad, G. (2002). Phagocytosis of dialysis-related amyloid deposits by macrophages. Nephrol. Dial. Transplant. *17*, 1136–1138.

Aslund, A., Herland, A., Hammarström, P., Nilsson, K.P., Jonsson, B.H., Inganäs, O., and Konradsson, P. (2007). Studies of luminescent conjugated polythiophene derivatives: enhanced spectral discrimination of protein conformational states. Bioconjug. Chem. *18*, 1860–1868.

Bankers-Fulbright, J.L., Kephart, G.M., Bartemes, K.R., Kita, H., and O'Grady, S.M. (2004). Platelet-activating factor stimulates cytoplasmic alkalinization and granule acidification in human eosinophils. J. Cell Sci. *117*, 5749–5757.

Boutet, S., and Williams, G.J. (2010). The Coherent X-ray Imaging (CXI) instrument at the Linac Coherent Light Source (LCLS). New Journal of Physics *12*, 035024.

Brünger, A.T. (1992). Free R value: a novel statistical quantity for assessing the accuracy of crystal structures. Nature *355*, 472–475.

David, K.K., Andrabi, S.A., Dawson, T.M., and Dawson, V.L. (2009). Parthanatos, a messenger of death. Front Biosci (Landmark Ed) *14*, 1116–1128.

Dereure, O., and Guilhou, J.J. (2002). [Eosinophilic-like erythema: a clinical subset of Wells' eosinophilic cellulitis responding to antimalarial drugs?]. Ann. Dermatol. Venereol. *129*, 720–723.

DiScipio, R.G., Khaldoyanidi, S.K., and Schraufstatter, I.U. (2011). Expression of soluble proteins in Escherichia coli by linkage with the acidic propiece of eosinophil major basic protein. Protein Expr. Purif. *79*, 72–80.

Dodson, G., and Steiner, D. (1998). The role of assembly in insulin's biosynthesis. Curr. Opin. Struct. Biol. *8*, 189–194.

Eisenberg, D., and Jucker, M. (2012). The amyloid state of proteins in human diseases. Cell *148*, 1188–1203.

Fowler, D.M., Koulov, A.V., Balch, W.E., and Kelly, J.W. (2007). Functional amyloid—from bacteria to humans. Trends Biochem. Sci. *32*, 217–224.

Frigas, E., and Gleich, G.J. (1986). The eosinophil and the pathophysiology of asthma. J. Allergy Clin. Immunol. *77*, 527–537.

Gilfillan, A.M., and Beaven, M.A. (2011). Regulation of mast cell responses in health and disease. Crit. Rev. Immunol. *31*, 475–529.

Gleich, G.J., Loegering, D.A., Mann, K.G., and Maldonado, J.E. (1976). Comparative properties of the Charcot-Leyden crystal protein and the major basic protein from human eosinophils. J. Clin. Invest. *57*, 633–640.

Goldschmidt, L., Teng, P.K., Riek, R., and Eisenberg, D. (2010). Identifying the amylome, proteins capable of forming amyloid-like fibrils. Proc. Natl. Acad. Sci. USA *107*, 3487–3492.

Hart, P., Boutet, S., Carini, G., Dubrovin, M., Duda, B., Fritz, D., Haller, G., Herbst, R., Herrmann, S., Kenney, C., et al. (2012). The CSPAD megapixel x-ray camera at LCLS. Proc. SPIE *8504*, 85040C, http://dx.doi.org/10.1117/12.930924.

Hartsel, S.C., and Weiland, T.R. (2003). Amphotericin B binds to amyloid fibrils and delays their formation: a therapeutic mechanism? Biochemistry *42*, 6228–6233.

Holgate, S.T. (2011). The sentinel role of the airway epithelium in asthma pathogenesis. Immunol. Rev. *242*, 205–219.

Kayed, R., Head, E., Thompson, J.L., McIntire, T.M., Milton, S.C., Cotman, C.W., and Glabe, C.G. (2003). Common structure of soluble amyloid oligomers implies common mechanism of pathogenesis. Science *300*, 486–489.

Kayed, R., Head, E., Sarsoza, F., Saing, T., Cotman, C.W., Necula, M., Margol, L., Wu, J., Breydo, L., Thompson, J.L., et al. (2007). Fibril specific, conformation dependent antibodies recognize a generic epitope common to amyloid fibrils and fibrillar oligomers that is absent in prefibrillar oligomers. Mol. Neurodegener. *2*, 18.

Kita, H. (2011). Eosinophils: multifaceted biological properties and roles in health and disease. Immunol. Rev. *242*, 161–177.

Lee, J.J., and Lee, N.A. (2005). Eosinophil degranulation: an evolutionary vestige or a universally destructive effector function? Clin. Exp. Allergy *35*, 986–994.

Leiferman, K.M., Ackerman, S.J., Sampson, H.A., Haugen, H.S., Venencie, P.Y., and Gleich, G.J. (1985). Dermal deposition of eosinophil-granule major basic protein in atopic dermatitis. Comparison with onchocerciasis. N. Engl. J. Med. *313*, 282–285.

Levy, M., Garmy, N., Gazit, E., and Fantini, J. (2006). The minimal amyloid-forming fragment of the islet amyloid polypeptide is a glycolipid-binding domain. FEBS J. *273*, 5724–5735.

Maji, S.K., Perrin, M.H., Sawaya, M.R., Jessberger, S., Vadodaria, K., Rissman, R.A., Singru, P.S., Nilsson, K.P., Simon, R., Schubert, D., et al. (2009). Functional amyloids as natural storage of peptide hormones in pituitary secretory granules. Science *325*, 328–332.

Miller, F., de Harven, E., and Palade, G.E. (1966). The structure of eosinophil leukocyte granules in rodents and in man. J. Cell Biol. *31*, 349–362.

Newsome, F. (1987). Suramin and eosinophil degranulation and vacuolation in onchocerciasis. Lancet *1*, 1381–1382.

Ohnuki, L.E., Wagner, L.A., Georgelas, A., Loegering, D.A., Checkel, J.L., Plager, D.A., and Gleich, G.J. (2005). Differential extraction of eosinophil granule proteins. J. Immunol. Meth. *307*, 54–61.

Oren, Z., Lerman, J.C., Gudmundsson, G.H., Agerberth, B., and Shai, Y. (1999). Structure and organization of the human antimicrobial peptide LL-37 in phospholipid membranes: relevance to the molecular basis for its non-cell-selective activity. Biochem. J. *341*, 501–513.

Otwinowski, Z., and Minor, W. (1997). Processing of X-ray Diffraction Data Collected in Oscillation Mode. In Methods in Enzymology, *Volume 276*, C.W. Carter, Jr. and R.M. Sweet, eds. (Academic Press), pp. 307–326.

Persson, T., Calafat, J., Janssen, H., Karawajczyk, M., Carlsson, S.R., and Egesten, A. (2002). Specific granules of human eosinophils have lysosomal characteristics: presence of lysosome-associated membrane proteins and acidification upon cellular activation. Biochem. Biophys. Res. Commun. *291*, 844–854.

Peters, M.S., Schroeter, A.L., and Gleich, G.J. (1983). Immunofluorescence identification of eosinophil granule major basic protein in the flame figures of Wells' syndrome. Br. J. Dermatol. *109*, 141–148.

Plager, D.A., Loegering, D.A., Weiler, D.A., Checkel, J.L., Wagner, J.M., Clarke, N.J., Naylor, S., Page, S.M., Thomas, L.L., Akerblom, I., et al. (1999). A novel and highly divergent homolog of human eosinophil granule major basic protein. J. Biol. Chem. *274*, 14464–14473.

Plager, D.A., Davis, M.D., Andrews, A.G., Coenen, M.J., George, T.J., Gleich, G.J., and Leiferman, K.M. (2009). Eosinophil ribonucleases and their cutaneous lesion-forming activity. J. Immunol. *183*, 4013–4020.

Ponikau, J.U., Sherris, D.A., Weaver, A., and Kita, H. (2005). Treatment of chronic rhinosinusitis with intranasal amphotericin B: a randomized, placebo-controlled, double-blind pilot trial. J. Allergy Clin. Immunol. *115*, 125–131.

Popken-Harris, P., Checkel, J., Loegering, D., Madden, B., Springett, M., Kephart, G., and Gleich, G.J. (1998). Regulation and processing of a precursor form of eosinophil granule major basic protein (ProMBP) in differentiating eosinophils. Blood *92*, 623–631.

Rosenberg, H.F., Dyer, K.D., and Foster, P.S. (2013). Eosinophils: changing perspectives in health and disease. Nat. Rev. Immunol. *13*, 9–22.

Sawaya, M.R., Sambashivan, S., Nelson, R., Ivanova, M.I., Sievers, S.A., Apostol, M.I., Thompson, M.J., Balbirnie, M., Wiltzius, J.J., McFarlane, H.T., et al. (2007). Atomic structures of amyloid cross-beta spines reveal varied steric zippers. Nature *447*, 453–457.

Sievers, S.A., Karanicolas, J., Chang, H.W., Zhao, A., Jiang, L., Zirafi, O., Stevens, J.T., Münch, J., Baker, D., and Eisenberg, D. (2011). Structure-based design of non-natural amino-acid inhibitors of amyloid fibril formation. Nature *475*, 96–100.

Simon, D., and Simon, H.U. (2007). Eosinophilic disorders. J. Allergy Clin. Immunol. *119*, 1291, 1300, quiz 1301–1302.

Simon, D., Hoesli, S., Roth, N., Staedler, S., Yousefi, S., and Simon, H.U. (2011). Eosinophil extracellular DNA traps in skin diseases. J. Allergy Clin. Immunol. *127*, 194–199.

Slungaard, A., and Mahoney, J.R., Jr. (1991). Thiocyanate is the major substrate for eosinophil peroxidase in physiologic fluids. Implications for cytotoxicity. J. Biol. Chem. *266*, 4903–4910.

Soscia, S.J., Kirby, J.E., Washicosky, K.J., Tucker, S.M., Ingelsson, M., Hyman, B., Burton, M.A., Goldstein, L.E., Duong, S., Tanzi, R.E., and Moir, R.D. (2010). The Alzheimer's disease-associated amyloid beta-protein is an antimicrobial peptide. PLoS ONE *5*, e9505.

Swaminathan, G.J., Weaver, A.J., Loegering, D.A., Checkel, J.L., Leonidas, D.D., Gleich, G.J., and Acharya, K.R. (2001). Crystal structure of the eosinophil major basic protein at 1.8 A. An atypical lectin with a paradigm shift in specificity. J. Biol. Chem. *276*, 26197–26203.

Thomas, L.L., Kubo, H., Loegering, D.J., Spillard, K., Weaver, A.J., McCormick, D.J., Weiler, C., and Gleich, G.J. (2001). Peptide-based analysis of amino acid sequences important to the biological activity of eosinophil granule major basic protein. Immunol. Lett. *78*, 175–181.

Torrent, M., Pulido, D., Nogués, M.V., and Boix, E. (2012). Exploring new biological functions of amyloids: bacteria cell agglutination mediated by host protein aggregation. PLoS Pathog. *8*, e1003005.

Treusch, S., Cyr, D.M., and Lindquist, S. (2009). Amyloid deposits: protection against toxic protein species? Cell Cycle *8*, 1668–1674.

Valent, P., Klion, A.D., Horny, H.P., Roufosse, F., Gotlib, J., Weller, P.F., Hellmann, A., Metzgeroth, G., Leiferman, K.M., Arock, M., et al. (2012). Contemporary consensus proposal on criteria and classification of eosinophilic disorders and related syndromes. J. Allergy Clin. Immunol. *130*, 607–612, e9.

Woschnagg, C., Rubin, J., and Venge, P. (2009). Eosinophil cationic protein (ECP) is processed during secretion. J. Immunol. *183*, 3949–3954.

Wright, B.L., Leiferman, K.M., and Gleich, G.J. (2011). Eosinophil granule protein localization in eosinophilic endomyocardial disease. N. Engl. J. Med. *365*, 187–188.

Yang, F., Lim, G.P., Begum, A.N., Ubeda, O.J., Simmons, M.R., Ambegaokar, S.S., Chen, P.P., Kayed, R., Glabe, C.G., Frautschy, S.A., and Cole, G.M. (2005). Curcumin inhibits formation of amyloid beta oligomers and fibrils, binds plaques, and reduces amyloid in vivo. J. Biol. Chem. *280*, 5892–5901.

Yousefi, S., Gold, J.A., Andina, N., Lee, J.J., Kelly, A.M., Kozlowski, E., Schmid, I., Straumann, A., Reichenbach, J., Gleich, G.J., and Simon, H.U. (2008). Catapult-like release of mitochondrial DNA by eosinophils contributes to antibacterial defense. Nat. Med. *14*, 949–953.

Molecular Cell

Supplemental Information

Toxicity of Eosinophil MBP Is Repressed by Intracellular Crystallization and Promoted by Extracellular Aggregation

Alice Soragni, Shida Yousefi, Christina Stoeckle, Angela B. Soriaga, Michael R. Sawaya, Evelyne Kozlowski, Inès Schmid, Susanne Radonjic-Hoesli, Sebastien Boutet, Garth J. Williams, Marc Messerschmidt, M. Marvin Seibert, Duilio Cascio, Nadia A. Zatsepin, Manfred Burghammer, Christian Riekel, Jacques-Philippe Colletier, Roland Riek, David S. Eisenberg, and Hans-Uwe Simon

SUPPLEMENTAL FIGURES

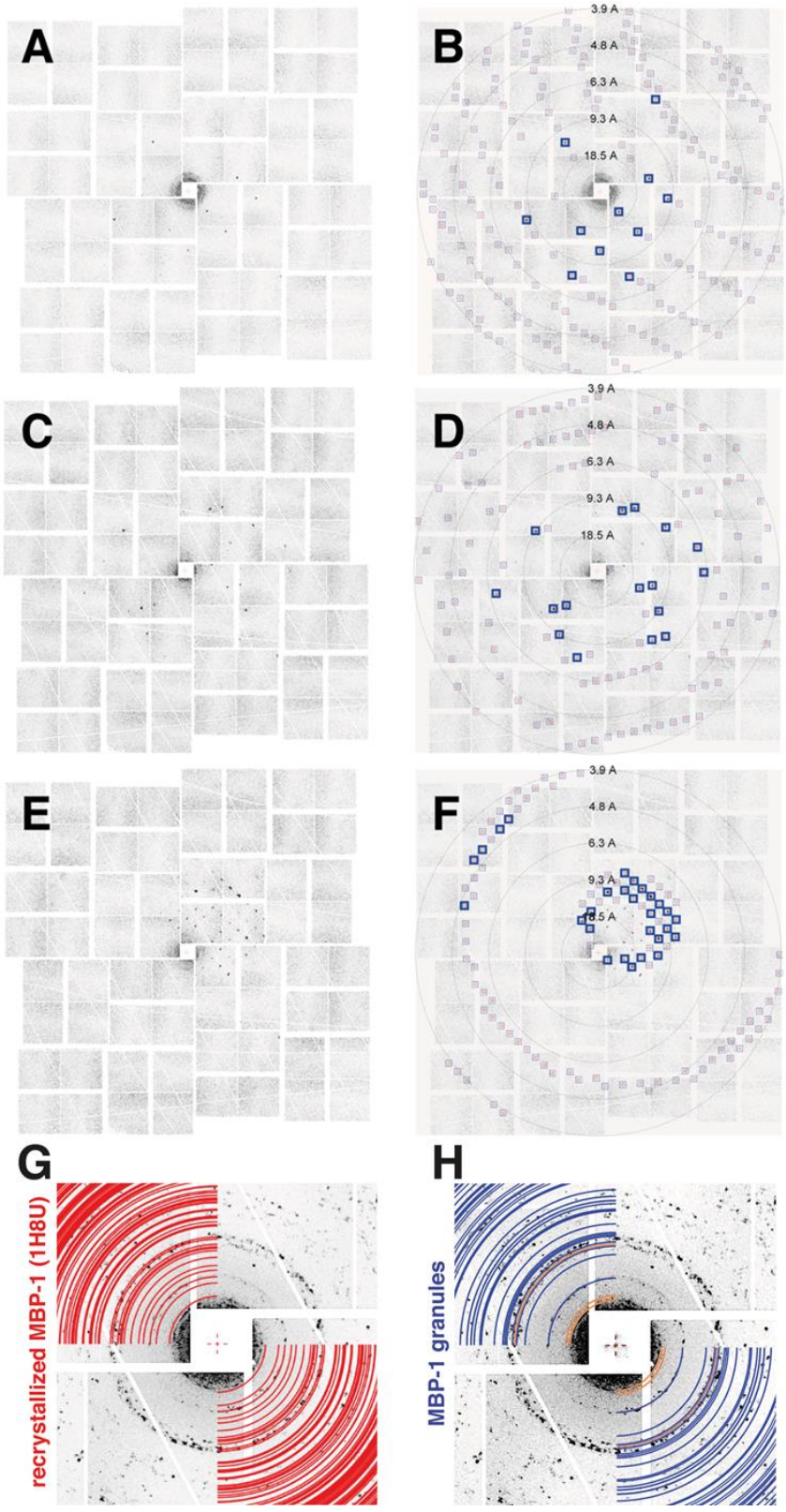

Figure S1. MBP-1 Nanocrystals Diffraction Obtained by XFEL Radiation and Comparison of Lattice Spacings of Purified and Recrystallized MBP-1 (related to Fig. 1)

(A, C, E) Diffraction patterns obtained from granule embedded MBP-1 single crystals by XFEL radiation.

(B, D, F) Diffraction patterns overlaid with predictions from the derived lattice constants. The blue boxes highlight those predicted diffraction spots which were observed experimentally. The detector is a mosaic of pixel array chips. The white lines at various angles trace the wire mask used for panel alignment, same as in Figure 1.

(G) Intragranular nanocrystals XFEL maximum projection overlaid with powder rings predicted from the recrystallized 1H8U cell. The observed diffraction from *in vivo* formed nanocrystals does not overlap with the recrystallized MBP-1, confirming substantial differences in the *in vivo* vs. *in vitro* packing.

(H) Intragranular nanocrystals XFEL maximum projection overlaid with powder rings predicted from the XFEL derived cell dimensions. The orange colored rings correspond to the 0,0,1; 0,1,0, and 1,0,0 reflections in order of increasing ring diameter. These reflections correspond to potential systematic absences and are key in determining whether the principle unit cell axes correspond to pure rotation symmetry or screw symmetry. The 0,0,1 reflection appears to be present. The 0,1,0 is absent. The presence or absence of 1,0,0 is uncertain. The XFEL derived spacings shown for a monoclinic cell would not differ significantly for an orthorhombic cell since the β angle is ~90°. (G) and (H) are zoomed in on the low resolution reflections. The edges of both images correspond to 17Å resolution. The maximum projection was obtained from 119 images.

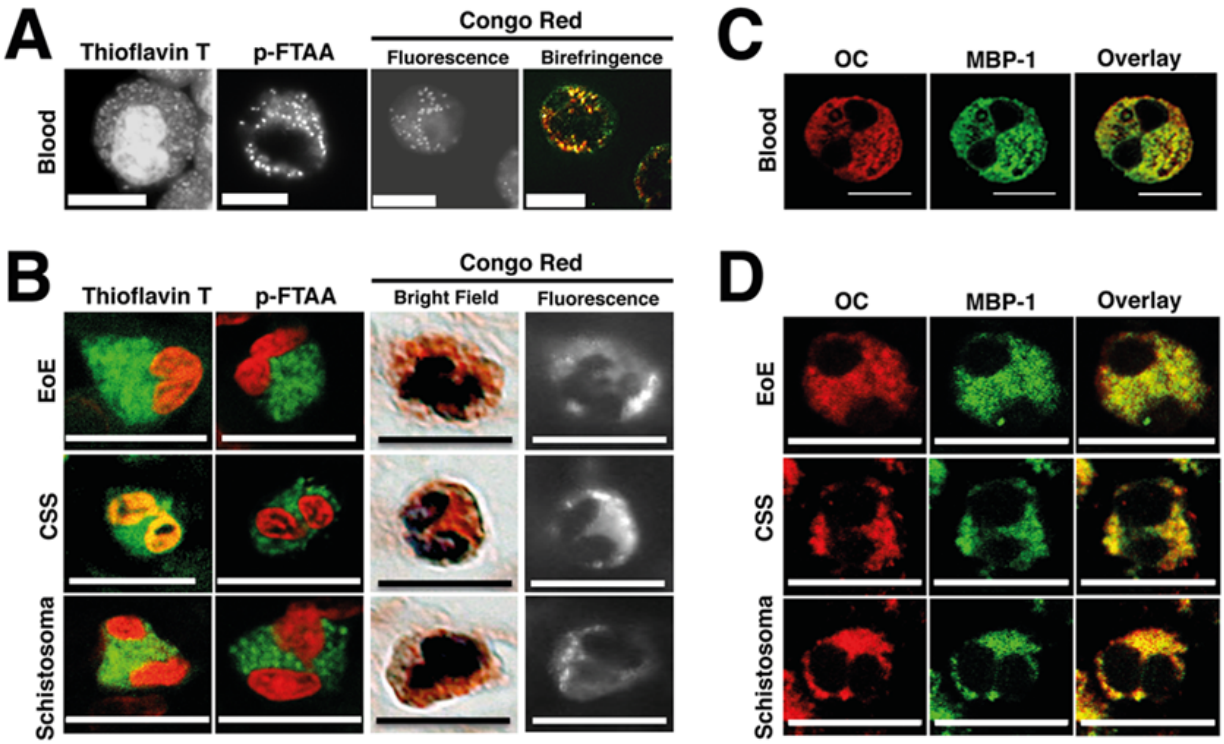

Figure S2. Tinctorial Properties of Eosinophil Granules (related to Fig. 1)
Blood (A) and tissue (B) eosinophils stained with Thioflavin T, p-FTAA and Congo Red. Blood eosinophils could be stained both supravitally as well as after formaldehyde fixation. Tissues were obtained from patients suffering from allergic (eosinophilic esophagitis, EoE; esophagus), autoimmune (Churg-Strauss syndrome, CSS; heart), and infectious diseases (Schistosoma; colon). Nuclei were counterstained with propidium iodide in the Thioflavin T and p-FTAA tissue eosinophil stains. Blood (C) and tissue (D) eosinophils were stained with the OC anti-amyloid aggregates and anti-MBP-1 antibodies. Scale bars: 10 μm.

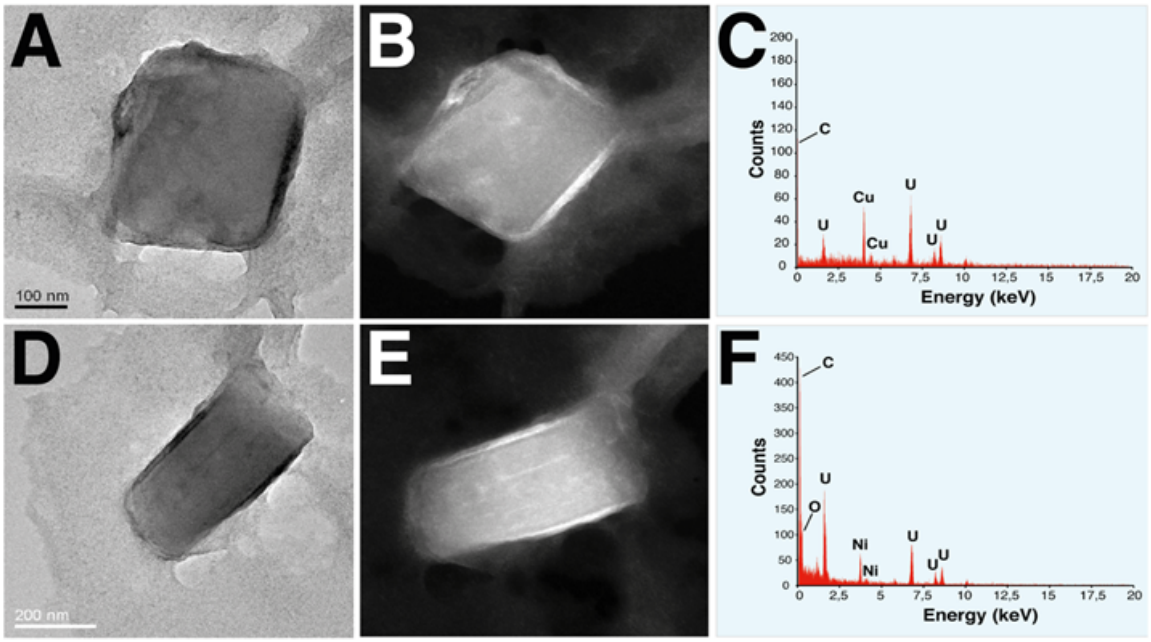

Figure S3. Absence of Heavy Metal Atoms In the Nanocrystalline MBP-1 Cores as Probed by *In Situ* Chemical Analysis (related to Fig. 1)

(A) Negatively stained isolated cores deposited on a carbon coated copper grid examined in bright field mode with a 300 kV TEM microscope. Scale bar: 100 nm.

(B) STEM image of the same core.

(C) STEM-EDX spectrum of the core shows mainly signals arising from the copper grid and the stain.

(D) Cores deposited on a nickel grid visualized in bright field mode. Scale bar: 200 nm.

(E) STEM image of the cores shown in panel D.

(F) The STEM-EDX spectrum shows signals arising from the nickel present in the grid and uranyl acetate from the staining procedure. The signals are labeled by atom type.

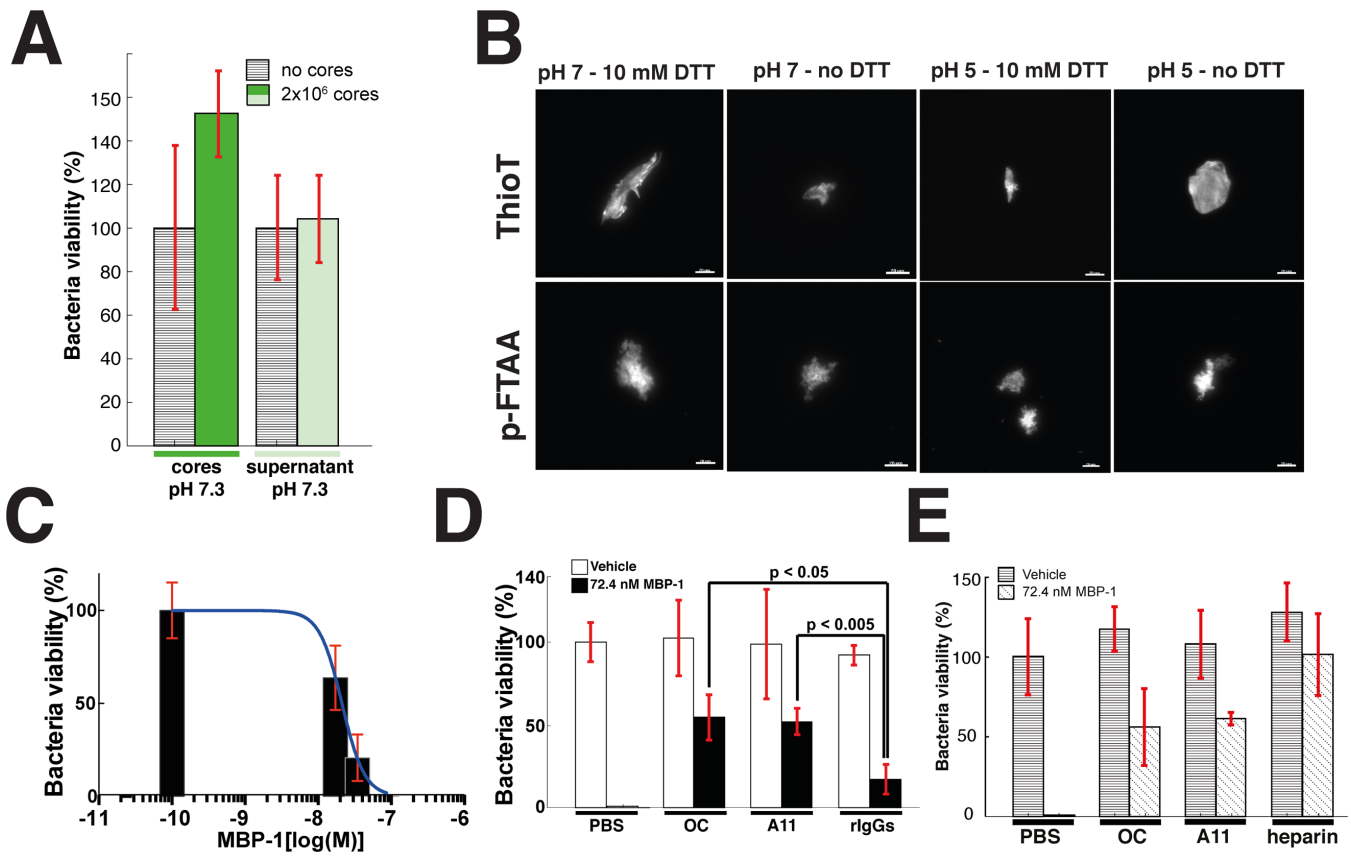

Figure S4. MBP-1 Toxicity Is Reduced by Heparin and Antibodies Specific to Amyloid Aggregates (related to Fig. 2, 3 and 4).

(A) Cores harvested from 2 x 10^6 eosinophils per condition were resuspended in PBS buffer, added to 0.5x10^7 *E. coli*/ml and incubated for 1 h before plating log-dilutions. Neither the entire cores nor the supernatant obtained upon centrifugation of the cores for 20 min at 20'000g exhibited any antibacterial activity.

(B) MBP-1 aggregates stained with the amyloid-specific dyes p-FTAA and Thioflavin T (ThioT). Scale bars: 20 µm.

(C) BKA. Purified MBP-1 was added to *E. coli* at the indicated concentrations. Data are normalized to the buffer control and are presented as mean levels ± % SD (bars) of one representative experiment. The red line represents the nonlinear fit which results in a calculated IC_{50} of ~18 nM.

(D) BKA to quantitate the observations reported in Figure 4A. OC and A11 antibodies significantly inhibited MBP-1 toxicity. Rabbit IgG was used as control.

(E) BKA. Addition of OC and A11 antibodies as well as heparin rescued bacterial viability indicating that interfering with the aggregation process is an effective mean to inhibit MBP-1 toxicity. Mean of three replicates ± % SD are shown.

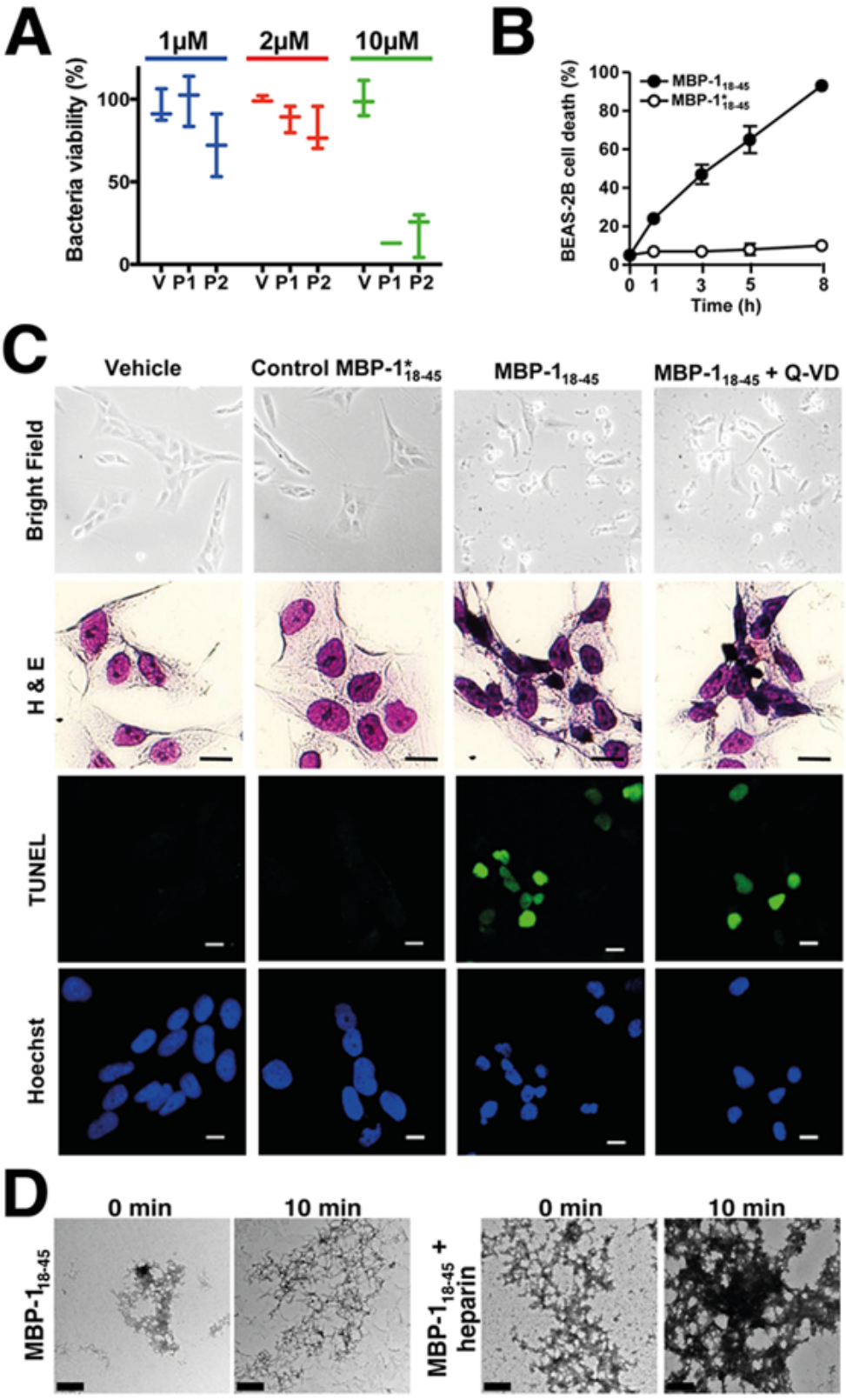
A
1μM
2μM
10μM
Bacteria viability (%)
100
50
0
V P1 P2 V P1 P2 V P1 P2
B
BEAS-2B cell death (%)
MBP-1 18-45
MBP-1* 18-45
100
80
60
40
20
0
0 1 3 5 8
Time (h)
C
Vehicle
Control MBP-1* 18-45
MBP-1 18-45
MBP-1 18-45 + Q-VD
Bright Field
H & E
TUNEL
Hoechst
D
0 min
10 min
0 min
10 min
MBP-1 18-45
MBP-1 18-45 + heparin

Figure S5. MBP-1 Peptide Toxicity Against Bacteria and Human Bronchial Epithelial BEAS-2B Cells (related to Fig. 4)

(A) BKA performed at three different concentrations of MBP-1_{18-45}: 1, 2 and 10 μM. Results for two different peptide batches are shown (P1, P2), while V indicates vehicle treatment (DMSO). Each peptide concentration value was normalized to the corresponding DMSO control. Median values for three replicates ± SEM are shown.

(B) Bronchial epithelial BEAS-2B cells were cultured with 5 μM MBP-1_{18-45} and control peptide for 5 h and analyzed in a time-dependent manner. Data are presented as mean levels ± SD of at least five independent experiments.

(C) Bronchial epithelial BEAS-2B cells were cultured with 5 μM MBP-1_{18-45} or control peptide for 5 h in the presence or absence of the apoptosis inhibitor Q-VD. The MBP-1 peptide induced a relatively round cell shape, loss of cell volume, and detachment as determined by bright field microscopy. Following H&E staining, nuclear condensation was additionally observed. The TUNEL assay indicated that the MBP-1 peptide induced DNA fragmentation, and Hoechst staining provided evidence for both nuclear condensation and nuclear fragmentation. The pharmacological inhibition of caspases, however, did not prevent the MBP-1-induced phenomena. All data are representative of three independent experiments. Scale bars: 10 μm.

(D) TEM of MBP-1_{18-45} aggregates obtained in the presence or absence of heparin. The effect of heparin on inactivation of toxicity can be mediated by the rapid aggregation process which converts toxic species into more inert fibrils.

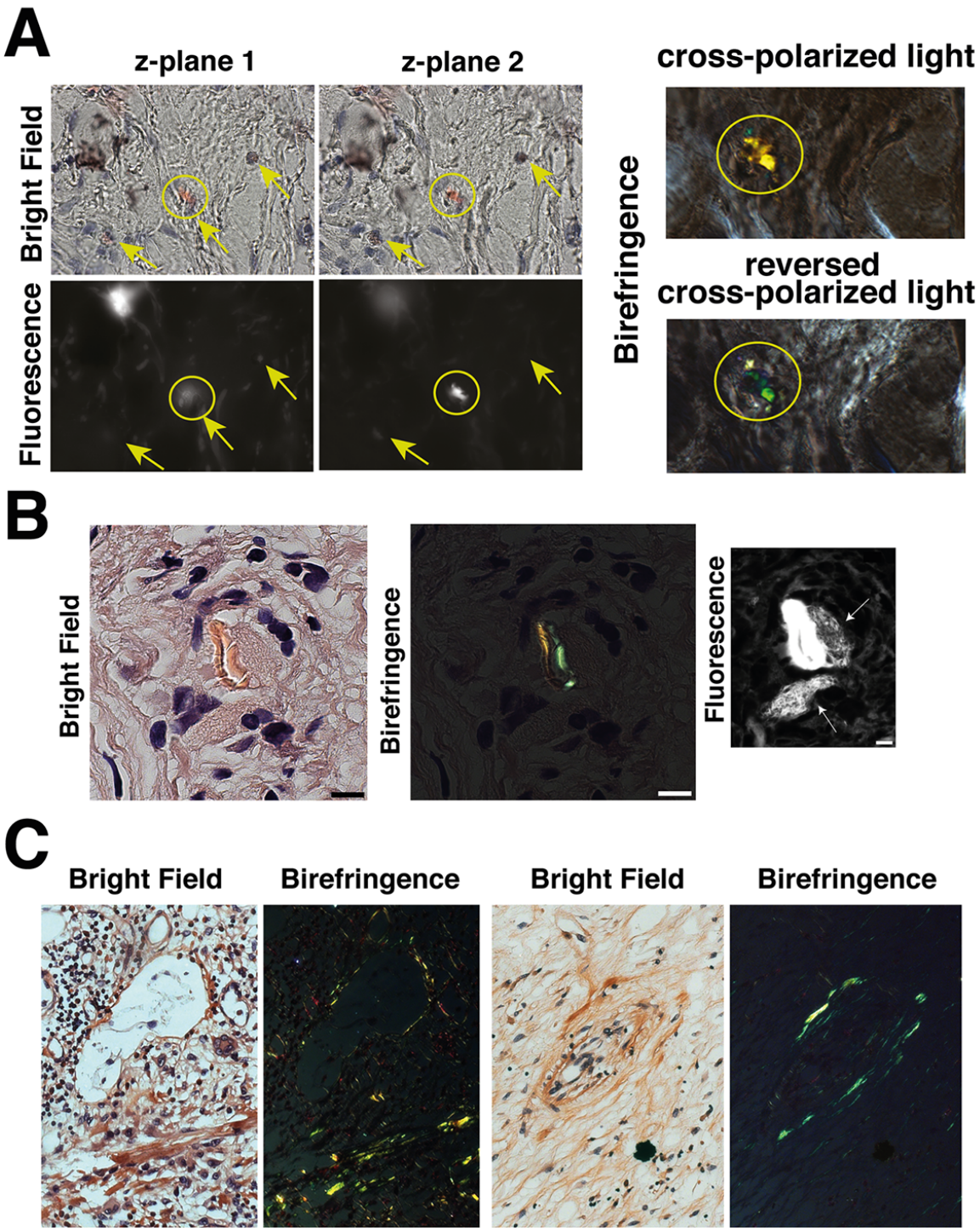
A
z-plane 1
z-plane 2
Bright Field
Fluorescence
cross-polarized light
Birefringence
reversed
cross-polarized light
B
Bright Field
Birefringence
Fluorescence
C
Bright Field
Birefringence
Bright Field
Birefringence

Figure S6. CR Stain of Tissue Biopsies of Patients With Eosinophil Related Diseases (related to Fig. 5)

(A) CR stain of skin tissue from an additional Wells' syndrome patient.
In the bright field and fluorescence mode it is possible to identify several eosinophils (arrows). An eosinophil is justapoxed to an amyloid deposit. This is evident changing the plane from z-plane 1, where the eosinophil is visible, to z-plane 2, where the amyloids are found. If the deposit is observed with cross-polarizers, the amyloid apple-green birefringence is evident. A yellow circle highlights the eosinophil and the extracellular deposit. The birefingent image is zoomed in to display the morphology of the amyloid plaque and confirms its extracellular nature.
(B) CR stain of skin tissue from an atopic dermatitis (AD) patient. Bright field and cross-polarized light images show positive apple green birefringent deposits surrounded by eosinophils. The birefringence is indicative of the presence of ordered amyloid fibrils. The CR fluorescence (right images) shows the presence of more amyloids deposited than visible with birefringence (additional regions highlighted by arrows). Scale bars are 10 μm for the bright field and polarized light images and and 5 μm for the fluorescence picture.
(C) CR stain of heart tissue from a Churg-Strauss Syndrome (CSS) patient.A post mortem evaluation of heart tissue shows extensive amyloid deposition visible as pale-red stained material in bright field mode and apple-green birefringent deposits under cross-polarized light. Magnification: 20x.

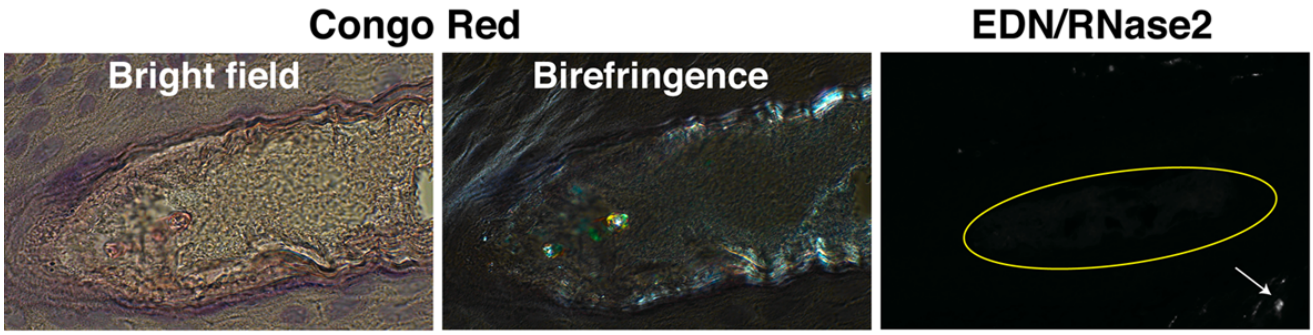

Figure S7. Wells' Syndrome Patient Exhibits Amyloid Deposition in Serial Sections of a Skin Biopsy (related to Fig. 5)

Congo Red stain of skin tissue from a serial section derived from the same sample as Figure 5. Amyloid deposits are stained red and exhibit apple green birefringence under cross-polarized light. These amyloid deposits are not constituted by EDN/RNase2 protein, as visible by the absence of EDN stain on the right, but contain MBP-1 protein (see Figure 5). The area containing the CR-positive amyloid deposit is indicated by a yellow circle while a positively EDN-stained eosinophil is indicated by an arrow. Magnification: 40x.

SUPPLEMENTAL TABLES

Table S1. Experimental Parameters for the XFEL Experiments Performed at LCLS CXI (related to Fig.1).

	LCLS CXI
X-ray focus (nm)	100 - 300
Wavelength (Å)	1.4674
Pulse energy (mJ)	1.125
Fluence at sample (ph*pulse)[a]	8.321×10^{11}
Dose (Ggy/crystal)[a]	2.0
Dose rate (Mgy/fs)[a]	33.3
Exposure time (s)	5×10^{-16}
Detector distance (mm)	230
Temperature (°C)	20
Pressure (torr)	10^{-5}
Shortest shot-to-shot distance (μm)	200[b]
Collection rate (frames/s)	0.2
Hit rate (%)	5.3

[a]Considering a 500x500x500 nm crystal
[b]Indicates only one shot per 200 x 200 μm window

Table S2. Unit Cell Parameters Predicted for Best Diffraction Patterns (related to Fig. 1)

Image	a	b	c	Reflections[a]
r0426_053622	26.636	54.760	58.214	146
r0425_053905	26.846	52.807	59.080	79
r0437_075428	25.765	53.175	59.024	84
r0437_080406	26.280	54.357	59.182	82
Average	26.382 +/- 0.473	53.775 +/- 0.932	58.875 +/- 0.445	

[a]Indicates the number of reflections indexed with I/sigma greater than 1.0

SUPPLEMENTAL EXPERIMENTAL PROCEDURES

Peptide Preparation and Crystallization

Peptide GNLVS (residues 26-30) was synthesized at greater than 97% purity (CS Bio, Menlo Park, CA) and dissolved in water at 20 mg/ml. Crystals were grown at 18°C via hanging-drop vapor diffusion in the presence of 0.1 M phosphate-citrate buffer at pH 4.2 and 2 M ammonium sulfate.

Data Collection and Structure Refinement

Crystals of segment GNLVS were mounted on the ends of pulled glass capillaries. Data was collected at 100 K using a microfocus beam (5x5 μm^2) at the 24-ID-E beamline of the Advanced Photon Source (APS) at Argonne National Laboratory. Data indexing, integration and scaling were performed using XDS/XSCALE (Kabsch, 1993) and DENZO/SCALEPACK (Otwinowski and Minor, 1997). The merged scaled data was imported into the CCP4 format by the programs organized under the "CCP4i" interface (Collaborative Computational Project, 1994). The molecular replacement solution for the segment was obtained using the program PHASER (Read, 2001), using a GAAVA beta-strand sequence as the search model (Murshudov et al., 1997). Crystallographic refinement was performed using PHENIX (Adams et al., 2010). Model building was done with COOT (Emsley and Cowtan, 2004) and illustrated with PYMOL (Delano, 2002).

MBP-1 Purification

Eosinophils were resuspended in 0.25 M sucrose with 250 U/ml of heparin and frozen until needed. Granules were extracted as described in the main text and directly used for protein purification. The proteins were extracted from the granules with 0.01 M HCl (Ohnuki et al., 2005). A Superdex 200 10/300 was equilibrated in 20 mM sodium acetate buffer with 150 mM NaCl at pH 4.2 and the protein mixture derived from the granules was injected at a flow rate of 0.5 ml/min.

The different peaks were run on a denaturing SDS-page gel and MBP-1 was identified from its apparent molecular weight as eluting at 1.4-column volumes, probably due to the strong interaction of the positively charged protein with the column resin. We additionally confirmed its identity by dot blot using an anti-MBP-1 antibody (BMK-13; ab48372, Abcam) and anti-mouse HRP-conjugated secondary antibody (Jackson ImmunoResearch).

Stain with Dyes

MBP-1 aggregates were deposited on a poly-lysine slide (Sigma). For the Thioflavin T staining, a drop of Thioflavin T solution (Sigma) (0.1-1 mM) was added directly on the slide and incubated for 1-2 min, then coverslipped and examined. For the p-FTAA staining, a drop of a 1:100 to 1:1000 p-FTAA dilution at a starting concentration of 1 mg/ml (courtesy of Dr. Andreas Åslund and Dr. Peter Nilsson, IFM, Linköping University, Linköping, Sweden) was added. Images were acquired using an epifluorescent Zeiss 200M (inverse) using the filters GFP-like Ex 485/20, Em 525/30 or TexasRed-like Ex 560/25, Em 607/36. The same protocols were followed for freshly isolated blood eosinophils and paraformaldehyde-fixed eosinophils. For the CR staining, a drop of CR solution from the HT60 kit (Sigma) was added to freshly isolated and formaldehyde-fixed eosinophils, incubated for 2 min, coverslipped and imaged with a Zeiss 200M equipped with double polarizing lenses.

The Thioflavin T, p-FTAA, and CR staining was also performed on 5-μm paraformaldehyde-fixed and paraffin-embedded tissue sections from patients with eosinophilic esophagitis (EoE; esophagus), Churg-Strauss syndrome (CSS; heart), and *Schistosoma* infection (colon). Thioflavin T and p-FTAA staining was performed as previously described (Sigurdson et al., 2007; Maji et al., 2009) and the fluorescence recorded with a laser-scanning confocal microscope (LSM 510, Carl Zeiss Microimaging). CR staining was performed using the HT60 kit according to manufacturer's instructions (Sigma) and images of stained tissues were acquired with a Zeiss 200M microscope.

MBP_{18-45} treatment of cells

20,000 cells were seeded on sterile glass coverslips in a 24-well tissue culture plate and allowed to adhere overnight. Next day, the medium was removed and cells were washed gently three times using DMEM containing 17 mM HEPES (pH 7.2-7.5), but no FBS. The peptides were then added to the cells and incubated for 5 h before fixation in 4% formaldehyde in PBS (pH 7.4), followed by washing three times in PBS. Staining was performed with Hoechst 33342 dye (1 µg/ml; Molecular Probes) for 5 min at room temperature after which the samples were washed three times with PBS, mounted on glass slides using Pro-Gold Mounting Medium (Life Biosciences), and visualized by confocal laser microscopy (LSM 510 Exciter, Carl Zeiss).

Viability Detection

Cell viability was measured after exposure to MBP-1 peptide or control peptide by means of ethidium bromide (1 µM) uptake and flow cytometry (FACS Calibur; BD Biosciences). For morphologic analysis, probes were stained with Diff-Quik dyes and analyzed with an Axiovert 35 microscope equipped with a 63x/numerical aperture 1.4, oil objective lens (Carl Zeiss, Jena, Germany).

Histologic Examination

5-µm tissue sections of human and mouse skin were stained with Hematoxylin & Eosin (H&E) and examined by light microscopy (Axiovert 35; Carl Zeiss).

SUPPLEMENTAL REFERENCES

Adams, P. D. *et al.* (2010). PHENIX: a comprehensive Python-based system for macromolecular structure solution. Acta Crystallogr. D Biol. Crystallogr. *66,* 213–221.

Collaborative Computational Project, Number 4. (1994). The CCP4 suite: programs for protein crystallography. Acta Crystallogr. D Biol. Crystallogr. *50,* 760–763.

Delano, W. (2002). The PyMOL Molecular Graphics System: http://www.pymol.org

Emsley, P., and Cowtan, K. (2004). Coot: model-building tools for molecular graphics. Acta Crystallogr. D Biol. Crystallogr. *60,* 2126–2132.

Kabsch, W. (1993). Automatic processing of rotation diffraction data from crystals of initially unknown symmetry and cell constants. J. Appl. Crystallogr. *26,* 795–800.

Maji, S. K. *et al.* (2009). Functional amyloids as natural storage of peptide hormones in pituitary secretory granules. Science *325,* 328-332.

Murshudov, G. N., Vagin, A. A., and Dodson, E. J. (1997). Refinement of macromolecular structures by the maximum-likelihood method. Acta Crystallogr. D Biol. Crystallogr. *53,* 240–255.

Ohnuki, L.E. *et al*. (2005). Differential extraction of eosinophil granule proteins. J. Immunol. Meth. *307,* 54-61.

Otwinowski, Z., and Minor, W. in *Methods Enzymol.* (Charles W., Carter, J.) Volume *276*, p. 307–326 (Academic Press, 1997).

Read, R. J. (2001). Pushing the boundaries of molecular replacement with maximum likelihood. Acta Crystallogr. D Biol. Crystallogr. *57,* 1373–1382.

Sigurdson, C. J. *et al*. (2007). Prion strain discrimination using luminescent conjugated polymers. Nat. Methods *4*, 1023–1030.